OPEN ACCESS Freely available online PLoS GENETICS

Id4, a New Candidate Gene for Senile Osteoporosis, Acts as a Molecular Switch Promoting Osteoblast Differentiation

**Yoshimi Tokuzawa[1☯], Ken Yagi[1☯], Yzumi Yamashita[1], Yutaka Nakachi[1], Itoshi Nikaido[1], Hidemasa Bono[1], Yuichi Ninomiya[1], Yukiko Kanesaki-Yatsuka[1], Masumi Akita[2], Hiromi Motegi[3], Shigeharu Wakana[3], Tetsuo Noda[3,4], Fred Sablitzky[5], Shigeki Arai[6], Riki Kurokawa[6], Toru Fukuda[7], Takenobu Katagiri[7], Christian Schönbach[8,9], Tatsuo Suda[1], Yosuke Mizuno[1], Yasushi Okazaki[1]*

1 Division of Functional Genomics and Systems Medicine, Research Center for Genomic Medicine, Saitama Medical University, Hidaka, Saitama, Japan, 2 Division of Morphological Science, Biomedical Research Center, Saitama Medical University, Iruma-gun, Saitama, Japan, 3 RIKEN BioResource Center, Tsukuba, Ibaraki, Japan, 4 The Cancer Institute of the Japanese Foundation for Cancer Research, Koto-ward, Tokyo, Japan, 5 Developmental Genetics and Gene Control, Institute of Genetics, University of Nottingham, Queen's Medical Center, Nottingham, United Kingdom, 6 Division of Gene Structure and Function, Research Center for Genomic Medicine, Saitama Medical University, Hidaka, Saitama, Japan, 7 Division of Pathophysiology, Research Center for Genomic Medicine, Saitama Medical University, Hidaka, Saitama, Japan, 8 Division of Genomics and Genetics, Nanyang Technological University School of Biological Sciences, Singapore, Singapore, 9 Department of Bioscience and Bioinformatics, Kyushu Institute of Technology, Iizuka, Fukuoka, Japan

Abstract

Excessive accumulation of bone marrow adipocytes observed in senile osteoporosis or age-related osteopenia is caused by the unbalanced differentiation of MSCs into bone marrow adipocytes or osteoblasts. Several transcription factors are known to regulate the balance between adipocyte and osteoblast differentiation. However, the molecular mechanisms that regulate the balance between adipocyte and osteoblast differentiation in the bone marrow have yet to be elucidated. To identify candidate genes associated with senile osteoporosis, we performed genome-wide expression analyses of differentiating osteoblasts and adipocytes. Among transcription factors that were enriched in the early phase of differentiation, Id4 was identified as a key molecule affecting the differentiation of both cell types. Experiments using bone marrow-derived stromal cell line ST2 and *Id4*-deficient mice showed that lack of *Id4* drastically reduces osteoblast differentiation and drives differentiation toward adipocytes. On the other hand knockdown of *Id4* in adipogenic-induced ST2 cells increased the expression of *Pparγ2*, a master regulator of adipocyte differentiation. Similar results were observed in bone marrow cells of femur and tibia of *Id4*-deficient mice. However the effect of *Id4* on *Pparγ2* and adipocyte differentiation is unlikely to be of direct nature. The mechanism of Id4 promoting osteoblast differentiation is associated with the Id4-mediated release of Hes1 from Hes1-Hey2 complexes. Hes1 increases the stability and transcriptional activity of Runx2, a key molecule of osteoblast differentiation, which results in an enhanced osteoblast-specific gene expression. The new role of Id4 in promoting osteoblast differentiation renders it a target for preventing the onset of senile osteoporosis.

Citation: Tokuzawa Y, Yagi K, Yamashita Y, Nakachi Y, Nikaido I, et al. (2010) Id4, a New Candidate Gene for Senile Osteoporosis, Acts as a Molecular Switch Promoting Osteoblast Differentiation. PLoS Genet 6(7): e1001019. doi:10.1371/journal.pgen.1001019

Editor: Gregory S. Barsh, Stanford University School of Medicine, United States of America

Received January 27, 2010; **Accepted** June 4, 2010; **Published** July 8, 2010

Funding: This work was supported by grants-in-aid of the Genome Network Project and Support Project of Strategic Research Center in Private Universities from the Ministry of Education, Culture, Sports, Science, and Technology (MEXT) to Saitama Medical University Research Center for Genomic Medicine. The funders had no role in study design, data collection and analysis, design, data collection and analysis, decision to publish, or preparation of the manuscript.

Competing Interests: The authors have declared that no competing interests exist.

* E-mail: okazaki@saitama-med.ac.jp

☯ These authors contributed equally to this work.

Introduction

Senile osteoporosis or age-related osteopenia is accompanied by increased bone marrow tissue adiposity [1]. Bone marrow adipocytes and osteoblasts are thought to originate from common mesenchymal stem cells (MSCs). Therefore, it has been suggested that the excessive accumulation of marrow adipocytes following bone loss is caused by unbalanced differentiation of MSCs into marrow adipocytes and osteoblasts [2]. Support for this hypothesis comes from studies of *peroxisome proliferators-activated receptor-γ* (*Pparγ*), a master regulator of adipocyte differentiation, deficient embryonic stem cells that showed an increase in osteoblast differentiation [3]. In contrast, calvarial adipocyte differentiation is augmented when *runt-related transcription factor 2 (Runx2)*, a master regulator of osteoblast differentiation has been knocked out [4]. Transcription factors Runx2 and *Sp7 transcription factor 7* (*Sp7*) regulate MSC commitment to osteoblast differentiation along with bone morphogenetic protein (BMP) signaling pathway [5]. Conversely, Pparγ and CCAAT/enhancer binding protein (C/EBP) transcription factor family members drive MSCs differentiation toward adipocytes [6]. Other proteins that regulate the balance between adipocyte and osteoblast differentiation are tafazzin, Wnt5a, Wnt10b, Msx2, C/EBPβ and basic helix-loop-helix (bHLH) family member e40 (Bhlhe40) [6–8]. Aforementioned transcription factors suppress adipocyte differentiation and promote osteoblast differentiation. Regardless of these studies, the precise molecular mechanisms that regulate the balance between osteoblast and adipocyte differentiation in the bone marrow has yet to be elucidated. Hence, we aimed to identify transcription factors that regulate the direction of differentiation toward osteoblast or adipocyte by analyzing their genome-wide expression profiles in differentiation time series experiments.

We noticed in early phases a subgroup of transcription factors that appeared to function in both osteoblasts and adipocytes differentiation. Particularly, bHLH superfamily transcription factors were significantly enriched and up-regulated in the early phase of osteoblast differentiation.

The bHLH superfamily comprises transcription factors that form homo- or heterodimers and typically bind to a consensus sequence (CANNTG) called an E-box [9]. It is well known that bHLH transcription factors play important roles in development and cell differentiation. For example, Myod1 is a key differentiation factor of myoblasts and Srebf1 is involved in adipocyte differentiation [10,11]. Hairy and enhancer of split (Hes) family members of bHLH superfamily are crucial regulators of cortical development [12].

Here, we have identified Inhibitor of DNA binding 4 (Id4), which also belongs to the bHLH superfamily as a key molecule that regulates the direction of differentiation toward osteoblast or adipocyte *in vitro* and *in vivo* using genome wide expression study. Furthermore, we established that Id4 promotes osteoblast differentiation by enhancing Runx2 transcriptional activity through stabilization of Runx2 protein. The new role of Id4 in directing osteogenic and adipogenic cell fate makes it a likely target for preventing the onset of senile osteoporosis.

Author Summary

Increased bone marrow adiposity is observed in the bone marrow of senile osteoporosis patients. This is caused by unbalanced differentiation of mesenchymal stem cells (MSCs) into osteoblast or adipocyte. Previous reports have indicated that several transcription factors play important roles in determining the direction of MSCs differentiation into osteoblast or adipocyte. So far, little is known about the overall dynamics and regulation of transcription factor expression changes leading to the imbalance of osteoblast and adipocyte differentiation inside the bone marrow. We have performed genome-wide gene expression analyses during the differentiation of MSCs into osteoblast or adipocyte. We identified basic helix-loop-helix transcription factor family member Id4 as a leading candidate controlling the differentiation toward adipocyte or osteoblast. Suppression of Id4 expression in MSCs repressed osteoblast differentiation and increased adipocyte differentiation. In contrast, overexpression of Id4 in MSCs promoted osteoblast differentiation and attenuated adipocyte differentiation. Moreover, *Id4*-mutant mice showed abnormal accumulation of lipid droplets in bone marrow and impaired bone formation activity. In summary, we have demonstrated a molecular function of Id4 in osteoblast differentiation. The findings revealed that Id4 is a molecular switch enhancing osteoblast differentiation at the expense of adipocyte differentiation.

Results

Genome-wide expression profile predicts *Id4* as a candidate molecular switch in osteoblast and adipocyte differentiation

To delineate the sequential changes of transcription factors activating and repressing downstream osteogenic and/or adipogenic target genes, we evaluated the differentiation capability toward both osteoblasts and adipocytes using six cell lines (ST2, C2C12, DFAT-D1, PA6, 10T1/2, NRG). Of these, bone marrow-derived stromal cell line ST2 differentiated most efficiently into both osteoblasts and adipocytes (data not shown). Using Affymetrix mouse GeneChip, we aimed to identify clusters of transcription factors that are temporally co-regulated in one but not in another cluster (CIBEX Accession number: CBX90). Of 1,270 transcription factors, 407 genes were significantly up- or down- regulated in either osteoblast or adipocyte differentiation compared to the non-induced control (Table 1 and Table S1). Hierarchical clustering analysis of transcription factor gene expression data at 15 osteoblast and seven adipocyte differentiation time points (Figure 1A) revealed distinct clusters that represent phases of sequentially expressed transcription factors (Figure 1B). Differentiation into osteoblasts is characterized by five phases (Figure S1) whereas adipocyte differentiation resulted in four phases (Table S1). The early phases of osteoblast (1 hr) and adipocyte (48 hr) differentiation showed the greatest variability in transcription factor expression levels (Figure 2A and Table S1).

Chi-square testing for over-representation of transcription factors in each differentiation phase supported only six up-regulated bHLH superfamily members (*Id1*, *Id2*, *Npas4*, *Id4*, *Hes1* and *Bhlhe40*) of the immediate early phase osteoblast differentiation (1 hr) as significantly ($p<0.01$) enriched (Figure 2B). Since *Id4*, *Hes1* and *Bhlhe40* expression increased (decreased) twofold or greater during osteoblast (adipocyte) differentiation compared to the control (Figure 2C and Table 2), these transcription factors are likely to play a pivotal role in the regulation of osteoblast and adipocyte differentiation.

Indeed, Hes1 and Bhlhe40 are known to be involved in both differentiation pathways [8,13,14], whereas Id4 has not yet been implicated in either differentiation pathways. Additionally, *Id4* expression patterns in osteoblast and adipocyte differentiation were also compared by quantitative real-time PCR (qRT-PCR). Expression of *Id4* significantly increased during osteoblast differentiation, attained a peak on day 4 and decreased thereafter (Figure S2A). In contrast, *Id4* expression decreased during adipocyte differentiation (Figure S2B). Expression levels of *Id1* and *Id2* were also up-regulated in the early stage (1 hr) of osteoblast differentiation, but thereafter their expression dropped

Table 1. Expression behavior of 1,270 transcription factors selected from all mouse genes (Ensembl release 52) based on GO IDs (Table 3) during osteoblast and adipocyte differentiation.

Transcription Factors		Osteoblast Differentiation				
		↑	↓	↑↓	~	Total
Adipocyte Differentiation	↑	22	6	4	70	102
	↓	25	40	21	132	218
	↑↓	3	5	2	2	12
	~	42	26	7	863	938
	Total	92	77	34	1,067	1,270

Arrows indicate up- (↑), down-regulated (↓), or up- and down-regulated (↑↓) transcription factors. No change in expression is symbolized by the almost equal sign (≈).

doi:10.1371/journal.pgen.1001019.t001

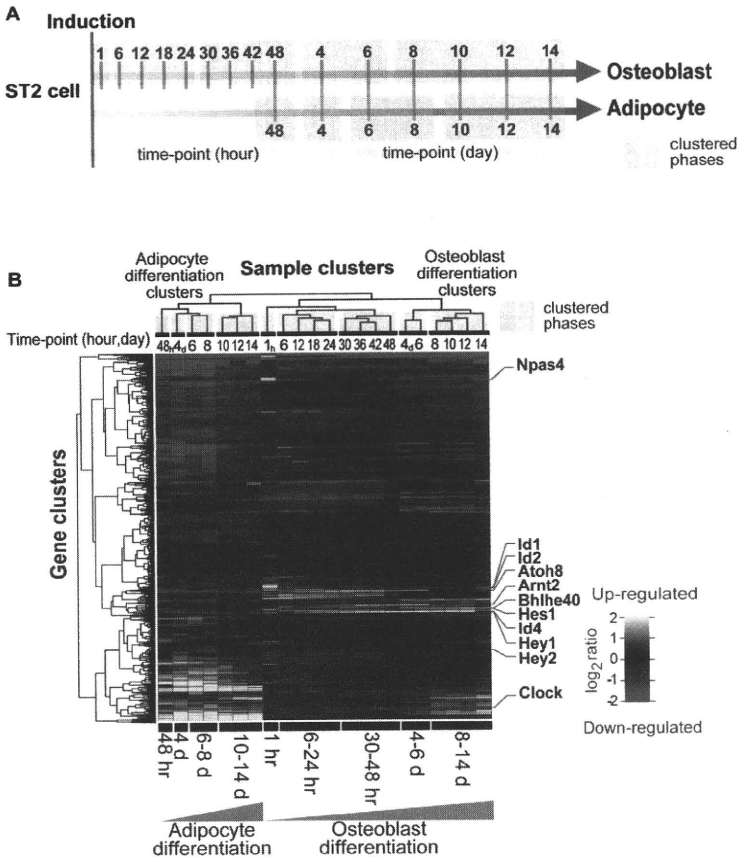

Figure 1. Transcription factor gene expression framework of differentiating ST2 cells. (A) Time-course sampling for gene expression analyses in ST2 cells. Vertical bars crossing the gradated blue and orange arrows indicate the sampling times during osteoblast and adipocyte differentiation, respectively. Five blue (osteoblasts) and four orange (adipocytes) boxes indicate the hierarchical clustering-derived phases of differentiation. (B) Gene expression heat map and clustering results of 1,270 transcription factors in 22 time-course samples.
doi:10.1371/journal.pgen.1001019.g001

to base levels (Figure 2C, upper panel). Therefore, we hypothesized that Id4 may act as a novel molecular switch in osteoblast and adipocyte differentiation.

Aside from *Id4*, *Hes1* and *Bhlhe40*, we identified additional bHLH members and various hypothetical and non-bHLH transcription factors as phase-specific candidate regulators of

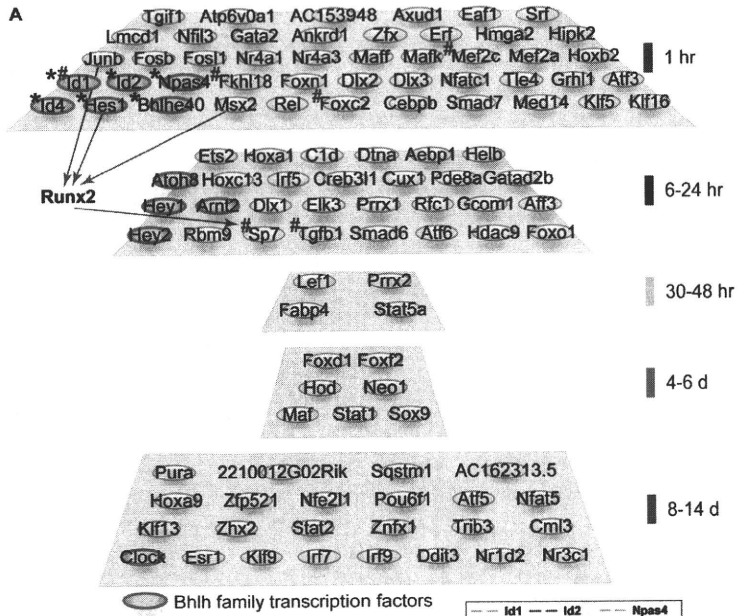

B

Observerd	Up-regulated at time point 1h	All genes other than up-regulated ones at 1h	Total no.
Bhlh family	6	106	112
All other genes	249	19,039	19,288
Total no.	255	19,145	19,400

Expected	Up-regulated at time point 1h	All genes other than up-regulated ones at 1h	Total no.
Bhlh family	1.47	110.53	112
All other genes	253.53	19,034.47	19,288
Total no.	255	19,145	19,400

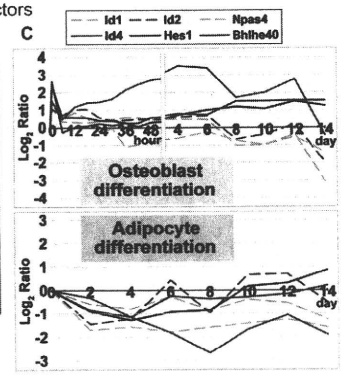

Figure 2. Enrichment of bHLH family in early phase of osteoblast differentiation and their expression pattern. (A) Summary of up-regulated transcription factors (Figure S1) associated with five phases of osteoblast differentiation. Asterisk (*): bHLH transcription factors that are overrepresented only during the early phase of osteoblast differentiation ($p<0.01$, Figure 2B). Sharp (#): transcription factors known to be associated with osteoblast differentiation and/or bone development. (B) Chi-square (χ^2) test for independence of bHLH superfamily genes in the immediate early phase (1 hr) of osteoblast differentiation. Null hypothesis: the occurrence of up-regulated bHLH transcription factors observed during the immediate early phase of osteoblast differentiation among all genes associated with probe set of Affymetrix GeneChip Mouse Genome 430 2.0 array is independent. Results of the contingency table (2×2 cells, degree of freedom = 1) allowed to reject the Null hypothesis. The expression of bHLH transcription factors was significantly up-regulated during the immediate early phase of osteoblast differentiation ($p<0.01$). (C) Expression pattern of six bHLH family genes in osteoblast and adipocyte differentiation. The chart represents expression changes of six bHLH genes during osteoblast and adipocyte differentiation. The horizontal axis indicates each time point after induction. The vertical axis indicates the logarithmic expression ratio (base 2) of each time point in comparison to the control (0 day).
doi:10.1371/journal.pgen.1001019.g002

osteo- and adipogenesis (Figure 2A and Table S1). The genes listed in Table S1 await further functional characterization regarding their involvement in osteoblast and/or adipocyte differentiation.

Id4 knockdown suppresses osteoblast differentiation of MSCs, and overexpression promotes osteoblast differentiation

To evaluate the potential role of Id4 in ST2 osteoblast differentiation, Id4 was suppressed by siRNA knockdown. As shown in Figure 3A, *Id4* siRNA (si*Id4*)-treated ST2 cells differentiating into osteoblasts showed a significant decrease in Id4 expression. The decline of *Id4* expression was accompanied by weak alkaline phosphatase (ALP) activity and reduced *bone γ carboxyglutamate protein 1* (*Bglap1* also called *osteocalcin*) expression (Figure 3B and 3C). Since both are markers of osteoblast differentiation, it appeared that Id4 is important in osteoblast differentiation of MSCs. We next evaluated whether forced expression of Id4 can promote osteoblast differentiation in MSCs by retroviral systems (Figure 3D). ST2 cells infected with Id4 recombinant retrovirus showed increased expression levels of *ALP* and *Bglap1* compared to cells infected with control virus independent of the presence or absence of BMP4 (Figure 3E and 3F). Taken together, Id4 promotes osteoblast differentiation of MSCs.

Id4 knockdown stimulates adipocyte differentiation, and overexpression attenuates lipid accumulation

Id4 knockdown in adipogenesis-induced ST2 cells (Figure 4A) significantly increased expression levels of other adipogenic marker genes such as *Pparγ2* [15] and *Adipoq* [16] (Figure 4B and 4C). Concomitantly, the number of Oil Red O stained lipid droplets and triglyceride levels also increased (Figure 4D and 4E). Forced expression of Id4 was confirmed by transfection into Cos7 cells with Id4 expression vector (Figure 4F). Adipocytes differentiated from ST2 cells transfected with Id4 expression vector showed slightly but significantly decreased lipid accumulation compared to empty vector transfectants (Figure 4G). The combined results of *Id4* siRNA knockdown and overexpression in ST2 suggest that Id4 attenuates differentiation of MSCs into adipocytes.

Id4-knockout mice ($Id4^{-/-}$) showed impaired osteoblast differentiation

Previously $Id4^{-/-}$ mice were studied only in context of neural development [17]. We confirmed that *Id4* expression was highest in the brain followed by cortical bone, kidney, thymus and bone marrow of C57BL/6J mice (Figure 5A). The body length and weight of 4 weeks old $Id4^{-/-}$ mice was 13–15% shorter and 35–40% lower compared to wild-type ($Id4^{+/+}$) littermates (Figure 5B and 5C). $Id4^{-/-}$ mice showed severe growth retardation and died by 5 weeks. In addition, we observed visible skeletal phenotypes of $Id4^{-/-}$ mice, but no skeletal deformities (data not shown). Altogether, our data hint at an important role of Id4 in bone formation.

Bone histological analysis of $Id4^{-/-}$ mice revealed significantly decreased bone volume (BV) in the 6th lumbar (Figure 5D and 5E).

Table 2. Expression of eleven bHLH transcription factors shown in Figure 2A.

	Differentiation		Differentiation Clusters	
Gene Symbol	**Osteoblast**	**Adipocyte**	**Osteoblast**	**Adipocyte**
Bhlhe40	↑	↓	1h ↑	4d ↓
Hes1	↑	↓	1h ↑	4d ↓
Id1	↑ ↓	↓	1h ↑	10d–14d ↓
Id2	↑ ↓	↓	1h ↑	2d ↓
Id4	↑	↓	1h ↑	4d ↓
Npas4	↑ ↓	↓	1h ↑	2d ↓
Arnt2	↑	≈	6h–24h ↑	≈
Atoh8	↑ ↓	↓	6h–24h ↑	2d ↓
Hey1	↑	≈	6h–24h ↑	≈
Hey2	↑	≈	6h–24h ↑	≈
Clock	↑	↑	8d–14d ↑	10d–14d ↑

Of eleven transcription factors, *Bhlhe40*, *Hes1* and *Id4* were two-fold or greater up-regulated during osteoblast differentiation. On the other hand, these genes were one-half fold or greater down-regulated during adipocyte differentiation. Arrows indicate up- (↑), down-regulated (↓), or up- and downregulated (↑ ↓) bHLH genes. No change in expression is symbolized by the almost equal sign (≈). Crosstalk functions between osteoblast and adipocyte differentiation have been reported for Bhlhe40 [8], Hes1 [13,14] and Id4 (this study), only.
doi:10.1371/journal.pgen.1001019.t002

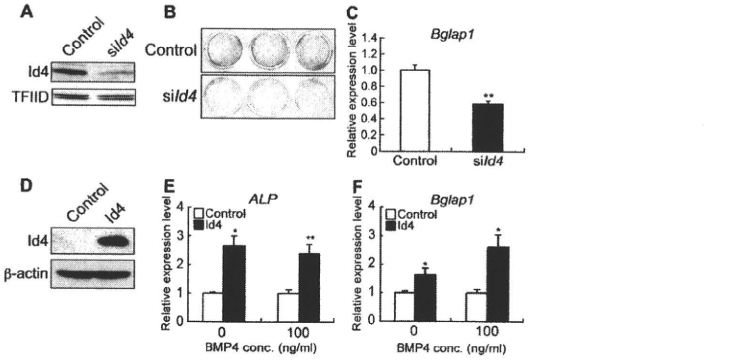

Figure 3. *Id4* promotes osteoblast differentiation in ST2 cells. (A) Western blotting of anti-Id4 antibody using ST2 nuclear extract. TFIID was detected as a loading control. Specific reduction of Id4 expression at day 2 after induction of ST2 cells treated with *Id4* siRNA (si*Id4*) for osteoblast differentiation. (B,C) Decrease in ALP activity (B) and *Bglap1* expression (C) at day 6 after induction of osteoblast differentiation in ST2 cells treated with si*Id4* as compared to the negative control. (D) Western blotting of anti-Id4 antibody using ST2 cell lysate, infected with Id4 retrovirus or control retrovirus (control). β-actin was detected as a loading control. (E,F) Increase in *ALP* (E) and *Bglap1* (F) expression at day 4 after infection with *Id4* virus as compared to the control virus in non-induced ST2 and ST2 osteoblast. Relative expression levels of *ALP* and *Bglap1* mRNA were measured by qRT-PCR. qRT-PCR data were subjected to Student's t-tests. Each error bar represents the mean ± SE of triplicates. *$p<0.05$ versus control, **$p<0.01$ versus control.
doi:10.1371/journal.pgen.1001019.g003

The bone formation rate (BFR) was decreased in $Id4^{-/-}$ mice compared to $Id4^{+/+}$ mice (Figure 5F and 5G). The BV to total volume ratio, BFR to bone surface (BS) ratio and mineral apposition rate (MAR) of $Id4^{-/-}$ mice were 57.3%, 28.1% and 30.7% lower compared to $Id4^{+/+}$ mice in the 6th lumbar, respectively (Figure 5N–5P).

In $Id4^{+/+}$ mice, active cuboidal-shaped osteoblasts (type II osteoblasts) were distributed in a row along the lumbar BS (Figure 5H), whereas in the corresponding region of $Id4^{-/-}$ mice osteoblasts were predominantly flat and resting (type IV osteoblasts; lining cells) (Figure 5I). The number of osteoblasts as a whole did not change significantly between $Id4^{+/+}$ and $Id4^{-/-}$ mice (data not shown). However, in $Id4^{-/-}$ mice the population of active osteoblasts was reduced (type II, Figure 5Q), whereas inactive osteoblasts accumulated (type IV, Figure 5R). These findings imply that Id4 modulates both differentiation of osteoblasts from pre-osteoblasts and regulation of osteoblast maturation.

Impaired bone formation was also observed in the lateral calvaria of $Id4^{-/-}$ mice (Figure 5K and 5M). In wild type mice, osteoblasts were closely lined up along the calvarial BS (Figure 5J). In contrast, no osteoblasts were observed along the calvarial bone of $Id4^{-/-}$ mice (Figure 5K). The osteoid thickness, BFR to BS ratios and MAR of $Id4^{-/-}$ mice calvarial bones were 61.5%, 49.1% and 65.2% of $Id4^{+/+}$ mice, respectively (Figure 5S, 5O, and 5P). These results suggest that Id4 is important for both endochondorial and membranous ossification. Growth Plate Width and Longitudinal Growth Rate (Lo. G. R) of $Id4^{-/-}$ mice tibia were 68.4% and 57.1% of $Id4^{+/+}$ mice, respectively (Figure S3A, S3B, S3C, S3D), which may have caused the growth retardation of $Id4^{-/-}$ mice.

Id4 interacts with Hey2 and inhibits the transcriptional repression of Hey2

Id family members are known to heterodimerize with other bHLH transcriptional factors, thus inhibiting the binding to the E-box motif [18]. To explore whether heterodimerized Id4 switches the direction of osteoblast and adipocyte differentiation, we assayed Id4 protein-protein interactions and analyzed their effects. Using immunoprecipitation we attempted to capture for candidate bHLH transcription factors that bind to Id4. Out of four tested bHLH transcription factors (Hes1, hairy/enhancer-of-split related with YRPW motif 1; Hey1, hairy/enhancer-of-split related with YRPW motif 2; Hey2 and Bhlhe40) (Figure S4A), only Hey2 bound to Id4 (Figure 6A, Figure S4A and S4B). An earlier study demonstrated that Hey2 is forming heterodimers with Hes1, which then bind to the E-box motif and repress transcription [19]. Therefore, we tested the effect of Id4 on transcriptional repression of Hey2/Hes1 heterodimers against the E-box element. Transcriptional repression onto E-box element in the presence of either Hey2 or Hes1 showed no effect or 39% inhibition of E-box transcriptional activity relative to control (empty expression vector), respectively (Figure 6B). Although luciferase activity was lowest in the presence of both Hey2 and Hes1, inhibition of transcriptional repression by Id4 increased in dose-dependent manner (Figure 6B). We also demonstrated that Hey2-Hes1 binding was abrogated with the dose-dependent increase of Id4 (Figure 6C, lane 5 and lane 6). Taken together, we confirmed that Id4 reverses the transcriptional repression by Hey2-Hes1 heterodimer in a dose-dependent manner.

Id4/Hey2 complex indirectly enhances Runx2 transcriptional activity

The presence of inactive osteoblasts (Figure 5I and 5R) in the bone tissues of the $Id4^{-/-}$ mice let us assume that Id4 may affect

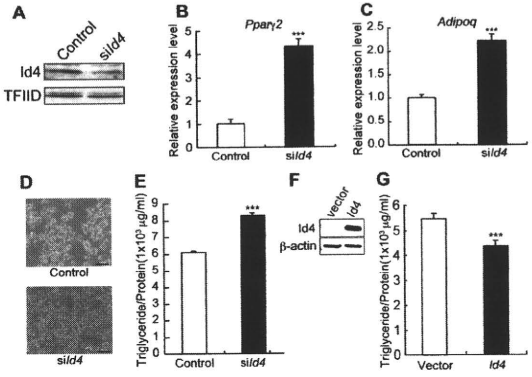

Figure 4. *Id4* weakly suppresses adipocyte differentiation in ST2 cells. (A) Western blotting of anti-Id4 antibody using ST2 nuclear extract. TFIID was detected as a loading control. Specific reduction of Id4 expression at day 2 after induction of ST2 cells treated with *siId4* for adipocyte differentiation. (B,C) Increase in *Pparγ2* (B) and *Adipoq* (C) expression at day 1 after induction of adipocyte differentiation and treatment with *siId4*. Relative expression levels of *Pparγ2* and *Adipoq* mRNA were measured by qRT-PCR. (D) Oil Red O staining of ST2 cells at day 4 after induction of adipocyte differentiation in presence of control or *siId4*. Original magnification: ×200; bar = 100 μm. (E) Lipid content of ST2 cells measured as triglyceride level at day 5 after adipogenic induction in presence of control or *siId4*. (F) Western blotting of anti-Id4 antibody using Cos7 cell lysate, transfected with Id4 expression vector or empty vector (Vector) as a control. β-actin was detected as a loading control. (G) Lipid content of ST2 cells transfected with Id4 expression vector or empty vector measured as triglyceride level at day 5 after adipogenic induction. qRT-PCR and lipid content data were subjected to Student's t-tests. Each error bar represents the mean ± SE of triplicates. *$p<0.05$ versus control and ***$p<0.005$ versus control.

doi:10.1371/journal.pgen.1001019.g004

the actions of Runx2 and Sp7, a key osteogenic differentiation molecule [20–22]. Osteoblast marker gene *Bglap1* expression level decreased not only in primary osteoblasts but also in embryonic day18.5 (E18.5) limb of $Id4^{-/-}$ mice (Figure S5A and S5B). *Bglap1*, a target gene of Runx2 has an E-box element other than osteoblast-specific element 2 (OSE2), which binds Runx2 to the promoter [23]. Therefore, we measured the promoter activity to examine the influence of Id4 on *Bglap1* E-box promoter-dependent transcriptional activity of Runx2. Although the suppression of *Bglap1* promoter activity by addition of Hes1 and Hey2 was not detected, a dose-dependent increase of transcriptional activity by Id4 was observed when testing the OSE2 element-containing promoter. When using the promoter without OSE2 the increase in transcriptional activity was not seen (Figure 7A). Since direct interaction between Id4 and Runx2 was ruled out experimentally (data not shown), Id4 may indirectly influence Runx2 transcriptional activity through Hes1. Hes1 is known to stimulate the transcriptional activity of Runx2 protein by increasing its stability during osteoblast differentiation [24]. We also confirmed that the addition of Hes1 stabilizes Runx2 protein. Interestingly, the addition of Id4 further increased the stabilization and accumulation of Runx2 (Figure 7B). Taken together, it appears that Id4 enhances Runx2 transcriptional activity through stabilization of Runx2 protein.

Taking into account the timing of the elevated *Id4* expression (Figure 2C and Figure S2A), our results strongly suggest that Id4 is indirectly driving the Hes1-mediated Runx2 stabilization during osteoblast differentiation. The facts that both Hes1 and Hey2 bind to the OSE2 element-containing *Bglap1* promoter region assessed by ChIP-qPCR, and that the amount of bound Hes1 and Hey2 decreased in ST2 osteoblasts (Figure 7C) further support this idea. However, the exact binding site of Hes1-Hey2 heterodimer remains to be identified. The proposed mechanism of Id4 action during osteoblast differentiation is illustrated in Figure 7D.

$Id4^{-/-}$ mice showed increased adipocytes

Id4 knockdown promoted adipocyte differentiation in ST2 cells (Figure 4B–4E). Histological analysis of $Id4^{-/-}$ tibia bones revealed elevated numbers of adipocytes in epiphyseal bone marrow of tibia compared to $Id4^{+/+}$ mice (Figure 8A–8D). The entire analyzed area of epiphyseal tibia bone marrow was occupied by adipocytes in $Id4^{-/-}$ mice (Figure 8E). Moreover, *Pparγ2* expression levels were also increased in bone marrow cells of femur and tibia of $Id4^{-/-}$ mice (Figure 8F). In comparison to $Id4^{+/+}$ mice, the number of adipocytes in the lateral calvaria was markedly increased in $Id4^{-/-}$ mice (Figure 5K). These aberrant traits observed in $Id4^{-/-}$ mice implicate Id4 as a crucial molecule in the lineage choice of MSCs differentiating into either osteoblasts or adipocytes (Figure 8G).

Discussion

In this study, we have delineated clusters of transcription factors that act as key regulators in the osteoblast and adipocyte differentiation network. The observation of sometimes disparately regulated transcription factors, led us to hypothesize a molecular

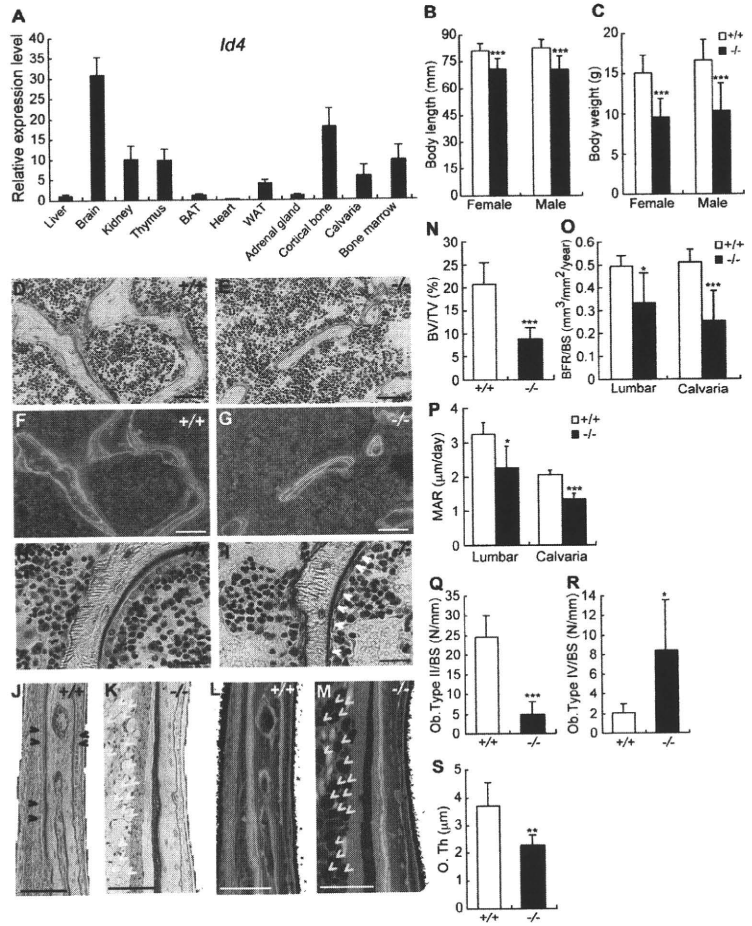

Figure 5. 4-week-old *Id4* knockout ($Id4^{-/-}$) mice show disturbance in growth and impaired osteoblast differentiation. (A) Tissue distribution of *Id4* mRNA in C57BL/6J male mice was measured by qRT-PCR. Brown adipose tissues; BAT, White adipose tissues; WAT. (B,C) Body length (B) and body weight (C) of wild-type ($Id4^{+/+}$) and $Id4^{-/-}$ mice. (D,E,H,I) Villanueva staining of the 6th lumbar bone of $Id4^{+/+}$ mice (D,H) and $Id4^{-/-}$ mice (E,I). Red and white arrowheads indicate active cuboidal-shaped osteoblasts (type II osteoblasts) and flattened resting osteoblasts (type IV

osteoblasts), respectively. (F,G,L,M) Bone formation rate (BFR) in the lumbar regions (F,G) and the lateral calvarial bone (L,M) of $Id4^{+/+}$ (F,L) and $Id4^{-/-}$ (G,M) mice. The BFR was measured using fluorescence microscopy following double-staining with tetracycline hydrochloride (blue arrowhead) and calcein (green arrowhead). Yellow arrowheads indicate adipocytes. (J,K) Villanueva staining of the lateral calvarial bone of $Id4^{+/+}$ (J) and $Id4^{-/-}$ mice (K). Black arrowheads indicate osteoblasts. The original magnifications and scale bars of the images are ×400 and 50 μm (D–G), ×400 and 30 μm (H,I) and ×200 and 50 μm (J–M). (N) Bone volume (BV) to total volume (TV) ratio in the 6th lumbar bone. (O,P) BFR to bone surface (BS) ratio (O) and mineral apposition rate (MAR) (P) in the 6th lumbar bone and lateral calvarial bone. (Q,R) Number of type II osteoblasts (Q) and type IV osteoblasts (R) on the corresponding area of the lumbar BS. (S) Osteoid thickness (O. Th) in the lateral calvarial bone. N-S: $Id4^{+/+}$ (n = 6), $Id4^{-/-}$ (n = 6). All data were subjected to Student's t-tests. Each error bar represents the mean ± SE. *$p<0.05$ versus control, **$p<0.01$ versus control and ***$p<0.005$ versus control.
doi:10.1371/journal.pgen.1001019.g005

switch function that promotes lineage-specific differentiation (e.g. osteoblast differentiation) and inhibits alternative differentiation pathways (e.g. adipocyte differentiation). To substantiate the hypothesis, we clustered gene expression profiles during osteoblast/adipocyte differentiation and identified Id4 as a candidate regulator of cell lineage choice. Id family members Id1–4 also belong to the bHLH superfamily, but lack the DNA binding domain. Heterodimerization of Id proteins with other bHLH proteins facilitates dominant negative regulation. A study by Bedford *et al.* using $Id4^{-/-}$ mice established Id4 as a regulator of proliferation and differentiation of neural precursor cells [17]. Until now, however, bone and skeletal abnormalities of this mouse model have not been reported. Besides our report, expression profile studies of BMP-independent osteoblast differentiation of human MSCs and BMP2-induced osteoblast differentiation using calvarial cells derived from Runx2-deficient mice [25,26] demonstrated that the expression level of *Id4* gene increases during osteoblast differentiation. These results suggest that Id4 plays an important role during osteoblast differentiation. Yet, the precise mechanism of Id4 action and regulation remained enigmatic. We have clearly demonstrated by *in vitro* and *in vivo* loss-of-function analysis that Id4 enhances osteogenic differentiation. Furthermore, we established a model of Id4 playing the role of molecular switch in osteoblast differentiation of MSCs (Figure 7D). Id4 expression increases upon BMP-induced osteoblast differentiation. Accumulating Id4 proteins transiently interact with Hes1-bound Hey2, thus triggering the release of Hes1 and the formation of Id4-Hey2 heterodimers and Hes1-Runx2 complexes. The binding of Hes1 to Runx2 potentiates the transcriptional activity of Runx2 and therefore osteoblast differentiation.

Hes1 and Hey2 are the target molecules of Notch signaling [19]. Until now, the relationship between Notch and BMP signaling pathways has been characterized by conflicting reports. On one hand experiments using ST2 cells showed that Notch1 suppresses the BMP-induced differentiation into osteoblasts [27]. On the other hand, Nobta et al. [28] reported that Notch signaling enhances BMP-induced osteoblast differentiation of C2C12 or MC3T3-E1 cells. At this point, there are insufficient data to resolve the controversy about the role of Notch signaling in BMP-induced osteoblast differentiation. However, our model (Figure 7D) may help to clarify the function of Notch signaling. In the absence of Id4, Hes1-Hey2 heterodimer just occupies the promoter region of the Runx2 target gene, whereas in the presence of Id4, Id4-Hey2 and Hes1-Runx2 complexes increase simultaneously. The concomitant increase of both complexes enhances the transcriptional activity of Runx2. Thus, we propose that availability and concentration of Id4 might account for the disparate roles of Notch signaling.

In $Id4^{-/-}$ mice, the drop of calvarial BFR is consistent with the phenotype of *Id1*/*Id3* heterozygous knockout mice. After BMP stimulation, *Id1*/*Id3* heterozygous knockout mice-derived calvarial cells showed reduced proliferation activity compared to calvarial cells derived from wild-type mice [29]. Thus, the decreased rate of calvarial bone formation in $Id4^{-/-}$ mice might be the consequence of reduced osteoblast proliferation. The expression levels of *Id1*and *Id2* were also up-regulated in the early stage of BMP4-induced osteoblast differentiation (Figure 2A). Indeed, it has been reported that *Id1* is an important early gene in osteoblasts after BMP stimulation [30,31]. Although the biological significance of Id1 in the regulation of MSCs has to be elucidated in future studies, in ST2 cells, expression levels of *Id1* and *Id2* immediately returned to base levels (Figure 2C). In contrast, *Id4* expression levels in ST2 and 3T3-E1 cells continued to rise until 4 days (Figure 2C and Figure S2A) and 7days, respectively [32].

Systemic hormones and local cytokines are known to be central regulators of bone formation. Serum levels of growth hormone (IGF1) and thyroid hormones (T3 and T4) did not change significantly between $Id4^{+/+}$ and $Id4^{-/-}$ mice (data not shown). Hence, impaired bone formation is most likely independent of hormonal factors and caused by repression of osteoblast differentiation.

Since the expression level of *Id4* decreases during adipocyte differentiation (Figure 2C and Figure S2B), Id4 was believed to inhibit MSCs differentiation into adipocytes. We demonstrated that Id4 suppression promoted adipocyte differentiation (Figure 4B–4E and Figure 8A–8E), but Id4 overexpression slightly decreased lipid accumulation level in ST2 adipocytes (Figure 4G). In an effort to shed light on the molecular mechanism, we assayed the expression level of *Pparγ2*, a master regulator of adipocyte differentiation. *Pparγ2* expression increased in adipogenic-induced ST2 cells when *Id4* was knocked down (Figure 4B) and in bone marrow cells of femur and tibia of $Id4^{-/-}$ mice (Figure 8F). However, the results of luciferase reporter assays ruled out effects of Id4 on the promoter activity of *Pparγ2* (data not shown). *Pparγ2* down-regulation by Id4 might involve a yet unknown, indirect regulatory mechanism. We noticed that the number of osteoclasts increased in the tibial epiphyseal regions and the 6th lumbar vertebra (data not shown). In view of an earlier report on Pparγ promoting osteoclast differentiation by activating *c-fos* [33], we interpret the increased number of adipocytes and osteoclasts in 6th lumbar and tibial bone of $Id4^{-/-}$ mice as a result of indirect activation of *Pparγ1* and/or *Pparγ2* transcriptional activity by lack of Id4. To corroborate these assumptions, additional analyses of the relationships and interactions of Id4, Pparγ and c-fos in context of adipocyte and osteoclast differentiation are necessary.

In summary, delineating clusters of transcription factors is a powerful strategy to identify cell fate-determining members of regulatory networks. Concerted application of our genome-wide expression profiling analyses and validation of transcription factor candidate regulators synthesize knowledge of specific molecular mechanism underlying osteoporosis and/or metabolic disease. In case of Id4, our findings reflect the potential pen-ultimate position of Id4 in the Runx2 activation/repression, which permits the differential integration of various upstream signals. Since BMP and Notch signaling affect osteoblast differentiation at different phases of differentiation, modulation of Id4 expression may create new venues for treating the onset of osteoporosis.

Materials and Methods

Cell culture

ST2 cells were obtained from RIKEN BioResource Center (BRC, Tsukuba, Japan) and cultured as described [34]. Primary

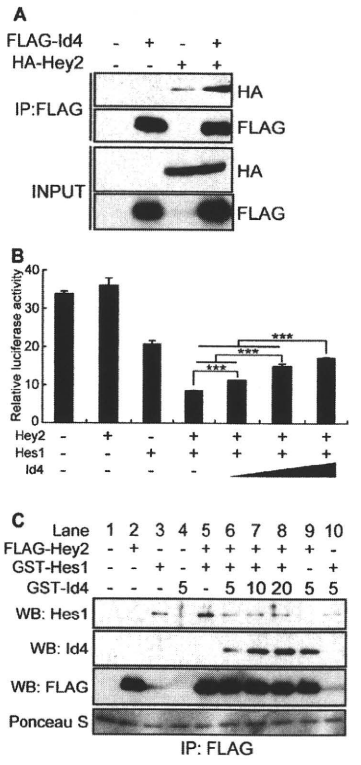

Figure 6. Id4 interacts with Hey2 and inhibits the suppression of reporter activity by Hey2/Hes1 complex. (A) Interaction of FLAG-tagged Id4 (FLAG-Id4) and human influenza hemagglutinin-tagged Hey2 (HA-Hey2) was confirmed in 293FT cells by immunoprecipitation (IP). (B) CV1 cells transfected with 6×E-box luciferase reporter, Hey2 and Hes1 expression vectors and with increasing doses of Id4 expression vector. Luciferase assay data were subjected to Student's t-tests. Each error bar represents the mean ± SE of triplicates. ***$p<0.005$ versus control. (C) *In vitro* assay of Id4 dose-dependent attenuation of Hey2-Hes1 complex interaction. GST-Id4 volume added was 5, 10 and 20 μl, respectively. WB: Western blotting.
doi:10.1371/journal.pgen.1001019.g006

osteoblasts were isolated from $Id4^{+/+}$ and $Id4^{-/-}$ neonatal calvarial bone as described previously [35]. Osteogenic differentiation was induced by changing the medium every three days to culture medium supplemented with 100 ng/ml of bone morphogenetic protein 4 (BMP4) (R&D Systems, Minneapolis, MN) and adipogenic differentiation was induced by changing the medium to differentiation medium supplemented with 10% fetal bovine serum (FBS), 0.5 mM 3-isobutyl-1-methlxanthine, 0.25 μM dexamethasone, and insulin-transferrin-selenium-X supplement containing 5 μg/ml of insulin (Invitrogen, Carlsbad, CA) and 1 μM rosiglitazone. After 48 hr, the differentiation medium was replaced with culture medium supplemented with 10% FBS.

Id4 knockdown by siRNA

siRNA sequences targeting the mouse Id4 transcript were purchased from Ambion (for adipocyte) and Invitrogen (for osteoblast). AllStar Negative Control siRNA (QIAGEN, cat. No., 1027281) and Negative Universal Control Med#2 (Invitrogen, cat. No., 12935-112) was used as a negative control in adipocyte and osteoblast differentiation, respectively. The sequences of siRNA used for Id4 knockdown were as follows; sense, CCUUUGUAUUUGAC-GUGUAtt; antisense, UACACGUCAAAUACAAAGGtt (Ambion, cat No. AM16704, ID. 159536); for adipocyte differentiation; sense, UUAAUUUCUGCUCUGGCCUCCCUU; antisense, AAGG-GAGGGCCAGAGCAGAAAUUAA (Invitrogen, stealth_455, cat No. 10620312); for osteoblast differentiation. For siRNA transfection, a complex of Lipofectamine 2000 (Invitrogen) and 20 nM siRNA was prepared according to the manufacturer's instruction and directly mixed with cells in the culture plates. The medium was replaced at 4–6 hr after transfection with fresh differentiation medium (adipogenic induction) or 10% FBS supplemented with 100 ng/ml of BMP4 (osteogenic induction).

Lipid assay and Alkaline phosphatase (ALP) staining

Lipid accumulation in adipocytes was detected by using Oil Red O staining as described previously [36]. The triglyceride content in adipocytes was determined as follows. ST2 cells were washed with cold phosphate-buffered saline (PBS) and total lipids were extracted with chloroform/methanol (2:1, v/v). The lower organic phase was dried, and the lipids were dissolved in 2-propanol. The triglyceride content was measured using Triglyceride E-test (Wako, Japan) according to the manufacturer's instructions. Protein concentrations were determined with Quick Start Bradford Dye Reagent (BIO RAD, 500-0205), using bovine gamma globulin as standard. ALP staining and measurements were performed as described previously [34].

Isolation of total RNA and quantitative real-time PCR (qRT–PCR)

Total RNA was isolated from liver, brain, kidney, thymus, brown adipose tissue (BAT), heart, white adipose tissue (WAT), adrenal gland, cortical bone, calvaria, bone marrow and posterior limb of E18.5 mouse embryo using TRIzol reagent (Invitrogen) and RNeasy columns (QIAGEN, Hilden, Germany) according to the manufacturer's instructions. Bone marrow was obtained by slicing of the ends of femur and tibia bones and then flushing it out with PBS using a syringe. Yield and quality of RNA were determined with a NanoDrop spectrometer (NanoDrop Technology, San Diego, CA) and a BioAnalyzer (Agilent Technologies, Santa Clara, CA). Gene expression levels were measured by qRT-PCR as described previously [34]. The sequences of forward and reverse primers used for each gene amplification were as follows; *gapdh*, GAPDH_768Fw_qPCR 5′-TGGAGAAACCTGCCAAG-TATG-3′, GAPDH_889Rv_qPCR 5′-GGAGACAACCTGGT-CCTCAG-3′; *Id4*, Mm_Id4_532Fw 5′-AGGGTGACAGCATT-CTCTGC-3′, Mm_Id4_658Rv 5′-CCGGTGGCTTGTTTC-TCTTA-3′; *Pparγ2*, PPARg2Fw 5′-ATGGGTGAAACTCTGG-

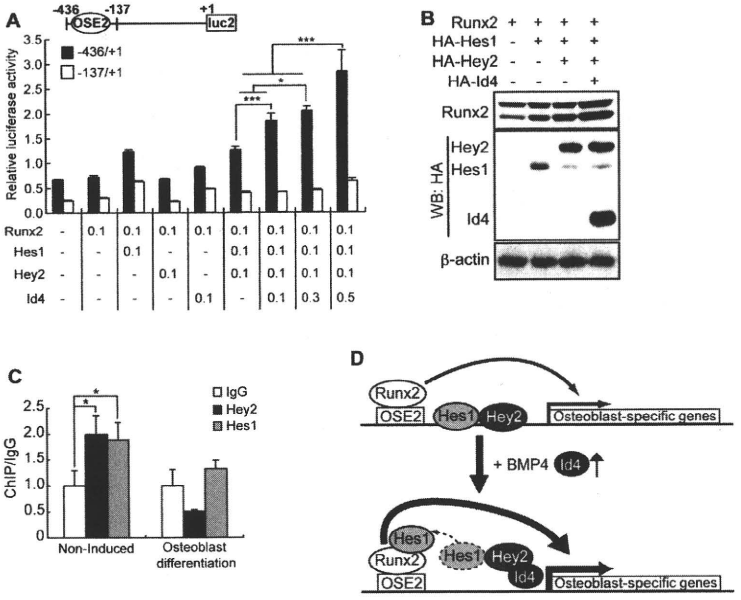

Figure 7. Id4 enhanced Runx2 transcriptional activity through stabilization of Runx2 protein. (A) Relative luciferase activity of *Bglap1* promoter in CV1 cells transfected with Runx2, Hes1, Hey2 and Id4 expression vectors. *Bglap1* promoter luciferase reporters were used as Runx2-dependent (−436bp/+1bp) or Runx2-independent (−137bp/+1bp). Luciferase assay data were subjected to Student's t-tests. Each error bar represents the mean ± SE of triplicates. *$p<0.05$ versus control and ***$p<0.005$ versus control. +1; transcription start site, bp; base pair. (B) Western blot analysis of Cos7 whole cell lysate using anti-Runx2, anti-HA and anti-β-actin (loading control) antibodies. The stability of Runx2-Hes1 complex increased in the presence of Id4. (C) ChIP-qPCR analyses of Hey2 and Hes1 binding onto *Bglap1* promoter in ST2 cells at day 4 after induction of osteoblast differentiation or non-induced ST2 cells. (D) A model of Id4 promoting Runx2-induced osteoblast differentiation.
doi:10.1371/journal.pgen.1001019.g007

GAGA-3′, PPARg2-1Rv 5′-GAGCTGATTCCGAAGTTGGT-3′; Bglap1, OC(PM15547142)Fw 5′-CTCTGTCTCTC TGAC-CTCACAG-3′, OC(PM15547142)Rv 5′-GGAGCTGCTGTGA-CATCCATAC-3′; *Adipoq*, Mm_AdipoQ_298Fw 5′-GATGG-CACTCCTGGAGAGAA-3′, Mm_AdipoQ_443Rv 5′-GCTTC-TCCAGGCTCTCCTTT-3′.

Expression microarray experiments

RNA was extracted from differentiating ST2 osteoblasts and adipocytes after induction of differentiation, using PureLink miRNA Isolation Kit (Invitrogen) according to the manufacture's instructions for total RNA purification. Total RNA derived from ST2 at 0 hr was used as control. Biotin-labeled cRNA was synthesized as recommended by Affymetrix guidelines. Labeled samples were hybridized to the Affymetrix GeneChip Mouse Genome 420 2.0 arrays according to the manufacturer's protocol. Scanning and intensity data analysis was preformed as described elsewhere [37].

Expression profiling analyses in ST2 osteoblast and adipocyte differentiation

Collected microarray expression data was background-subtracted, and normalized using the robust multi-array analysis method [37]. Differentially expressed genes were determined by selecting expression subgroups that contained the probe sets of up/down-regulated genes. Genes were considered up-regulated (down-regulated) if their $\log_2$ intensity ratio was greater (less) than 1 (−1), or greater (less) than the mean plus (minus) 3-times standard deviation. All gene and probe set annotations were derived from Ensembl release 52. Genes with transcription-related Gene Ontology (GO) annotations (Table 3) were considered as transcription factor-coding genes. Genes with InterPro accession IPR001092 were annotated as bHLH transcription factor-coding genes. Spotfire DecisionSite version 8.1.1 (TIBCO Software, Inc.) was used for hierarchical clustering and generating the gene expression heat maps.

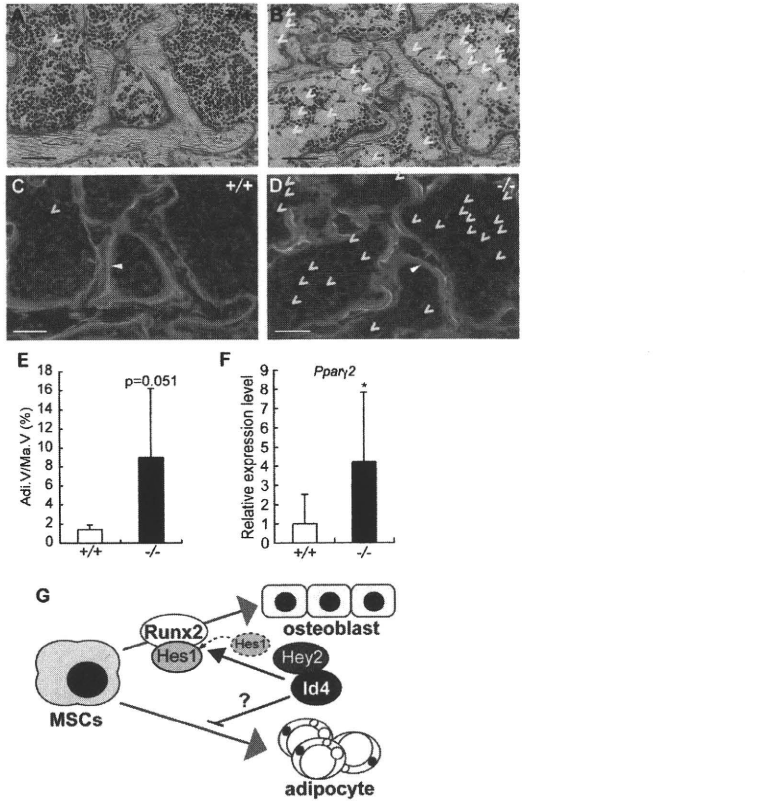

Figure 8. 4-week-old *Id4*$^{-/-}$ mice show increased adipocytes in bone marrow. (A,B) Villanueva staining of epiphyseal tibia of *Id4*$^{+/+}$ (A) and *Id4*$^{-/-}$ mice (B). (C,D) The BFR was measured in the tibial epiphysial regions in *Id4*$^{+/+}$ (C) and *Id4*$^{-/-}$ mice (D) using a fluorescence microscopy following double-staining with tetracycline hydrochloride (blue arrowheads) and calcein (white arrowheads). Yellow arrowheads indicate adipocytes. The original magnifications and scale bars of the images are ×400 and 100 μm. (E) The total area occupied by adipocytes (Adi.V) in the epiphyseal tibia bone marrow. *Id4*$^{+/+}$ (n = 6), *Id4*$^{-/-}$ (n = 6). (F) *Pparγ2* mRNA expression is significantly elevated in bone marrow cells of *Id4*$^{-/-}$ compared to *Id4*$^{+/+}$ mice. Relative expression levels of *Pparγ2* mRNA were measured by qRT-PCR. *Id4*$^{+/+}$ (n = 9), *Id4*$^{-/-}$ (n = 10). All data were subjected to Student's t-tests. Each error bar represents the mean ± SE. *$p<0.05$ versus control. (G) The role of Id4 in bone formation and bone marrow environment.
doi:10.1371/journal.pgen.1001019.g008

Luciferase reporter assays

Bglap1 promoter regions were cloned by PCR from the mouse genome. 6×E-box sequence (CGCGTCCACGTGGGGCCAC-GTGGGGCCACGTGGGCCACGTGGG GCCACGTGGG-

Table 3. Gene ontology IDs and terms (GO release 2009-01-25) associated with 1,270 transcription factors of Table 1.

GO ID	GO Term
GO:0000156	two-component response regulator activity
GO:0003700	transcription factor activity
GO:0003701	RNA polymerase I transcription factor activity
GO:0003702	RNA polymerase II transcription factor activity
GO:0003704	specific RNA polymerase II transcription factor activity
GO:0003705	RNA polymerase II transcription factor activity, enhancer binding
GO:0003706	ligand-regulated transcription factor activity
GO:0003709	RNA polymerase III transcription factor activity
GO:0003711	transcription elongation regulator activity
GO:0003712	transcription cofactor activity
GO:0003713	transcription coactivator activity
GO:0003714	transcription corepressor activity
GO:0003715	transcription termination factor activity
GO:0003716	RNA polymerase I transcription termination factor activity
GO:0003717	RNA polymerase II transcription termination factor activity
GO:0003718	RNA polymerase III transcription termination factor activity
GO:0008140	cAMP response element binding protein binding
GO:0008148	negative transcription elongation factor activity
GO:0008159	positive transcription elongation factor activity
GO:0016251	general RNA polymerase II transcription factor activity
GO:0016252	nonspecific RNA polymerase II transcription factor activity
GO:0016455	RNA polymerase II transcription mediator activity
GO:0016563	transcription activator activity
GO:0016564	transcription repressor activity
GO:0016565	general transcriptional repressor activity
GO:0016566	specific transcriptional repressor activity
GO:0016943	RNA polymerase I transcription elongation factor activity
GO:0016944	RNA polymerase II transcription elongation factor activity
GO:0016945	RNA polymerase III transcription elongation factor activity
GO:0016986	transcription initiation factor activity
GO:0016987	sigma factor activity
GO:0016988	transcription initiation factor antagonist activity
GO:0016989	sigma factor antagonist activity
GO:0017163	negative regulator of basal transcription activity
GO:0030374	ligand-dependent nuclear receptor transcription coactivator activity
GO:0030375	thyroid hormone receptor coactivator activity
GO:0030401	transcription antiterminator activity
GO:0030528	transcription regulator activity
GO:0042156	zinc-mediated transcriptional activator activity

doi:10.1371/journal.pgen.1001019.t003

GCCACGTGGGGA) and cloned fragments were ligated to the firefly luciferase gene (derived from pGL4.10, Promega). CV1 cells were co-transfected with the firefly luciferase reporter vectors, expression vectors and the internal control Renilla luciferase vector (pGL4.74, Promega) using Lipofectamine 2000 (Invitrogen). Luciferase activities were measured with Wallac 1420 Multilabel counter (PerkinElmer Life and Analytical Sciences, Turku, Finland). These experiments were performed in triplicate.

Co-immunoprecipitation and GST–pull down assay

Cos7 cells were transfected with FLAG-Id4 expression vector with either HA tagged expression vector (Hes1, Hey1, Hey2, Bhlhe40). The extracts from the transfected cells were incubated with Protein G sepharose beads and precipitated with either anti-FLAG antibody (SIGMA) or normal mouse IgG (Santa cruz) overnight at 4C°. After washing with PBS, bound proteins were separated by SDS-PAGE followed by Western blot analysis with anti-HA antibody, anti-FLAG antibody. GST-Id4 expression vector, Flag-Hey2 expression vector and Flag-empty vector were expressed in *E.coli*. The crude extract of GST-Id4 or GST expressed in *E.coli* was incubated with glutathione sepharose beads for 4 hr at 4C°. The precipitate was incubated with the extract of Flag-Hey2 overnight at 4C°. After washing, the bound proteins were separated by SDS-PAGE followed by Western blot analysis with anti-Flag antibody.

Chromatin Immunoprecipitation (ChIP)–qPCR analysis

ChIP was performed as described previously [38]. ST2 cells were cultured for 4 days with or without 100 ng/ml BMP4, respectively. The antibodies used for ChIP were anti-Hey2 (Protein Tech Group, cat No. 10597-1-AP), anti-Hes1 (Santa Cruz, H-140) and normal rabbit IgG (Santa Cruz, sc-2027) as negative control. Forward and reverse qPCR primer sequences contained OSE2 of the *Bglap1* promoter (Bglap2_ChIP_L789, 5′-GATTGTGGCCTCTCGTC-3′;Bglap2_ChIP_R8, 5′- ATCG-GCTACTCTGTGCTCT-3′).

Animals

Id4$^{-/-}$ mice previously generated by Bedford et al. (2005) were kindly supplied by Dr. Kondo who received them originally from Dr. Sablitzky (University of Nottingham). All mice used in this study were maintained and handled according to the protocols approved by the Animal Research Committee of Saitama Medical University.

Bone morphometric measurements

To assess the static and dynamic parameters of bone histomorphometry, 3 weeks old female mice were labeled with intraperitoneal injections of 20 mg/kg of tetracycline hydrochloride (Sigma) at 4 days before sacrifice. Two days before sacrifice, the mice were injected with 10 mg/kg of calcein (Dojindo Co., Kumamoto, Japan). Tibiae and lumbar vertebrae were removed from each mouse, and fixated with 70% ethanol. The bones were trimmed to remove the muscle, stained with Villanueva bone stain for 5 days, dehydrated in graded concentrations of ethanol, and embedded in methyl-methacrylate (Wako Chemicals, Kanagawa, Japan) without decalcification. Sagittal plane sections (5 μm thick) of the lumbar vertebrae were cut using a Microtome (Leica, Germany). Bone morphometric analyses were performed using a semi-automatic image analyzing system software (System Supply, Nagano, Japan) and Optiphot fluorescent microscope (Nikon, Tokyo, Japan).

Supporting Information

Figure S1 Heat-map of osteoblast differentiation phase-specific up-regulated transcription factor genes. Transcription factors of the bHLH family are indicated by purple bars. The column 'Cluster groups' shows the gene symbols of up-regulated transcription factors in time-sequential (chronological) cluster order. The gene symbols of the up-regulated transcription factors are listed in the same order as they appear on the image. Phase 1 (1hr; 46 transcription factors): Foxc2, Nfatc1, Hoxb2, Fkhl18, Med14, Id4, Msx2, Id2, Ankrd1, Hes1, Bhlhe40, Foxn1, Tle4, Hmga2, Dlx3, Gata2, Dlx2, Nr4a3, Axud1, Eaf1, Hipk2, AC153948.5, Zfx, Cebpb, Grhl1, Smad7, Rel, Maff, Mafk, Klf16, Id1, Nfil3, Fosl1, Klf5, Npas4, Lmcd1, Atf3, Fosb, Mef2c, Erf, Mef2a, Atp6v0a1, Srf, Tgif1, Nr4a1 and Junb; phase 2 (6–24hr; 29 transcription factors); Hey1, Atoh8, Helb, Hdac9, Atf6, Gcom1, Hoxa1, Prrx1, Tgfb1, Creb3l1, Rbm9, Elk3, C1d, Dlx1, Pde8a, Hey2, Ets2, Dtna, Smad6, Foxo1, Cux1, Gatad2b, Irf5, Rfc1, Sp7, Arnt2, Acbp1, Hoxc13 and Aff3; phase 3 (30–48hr; 4 transcription factors): Lcf1, Fabp4, Stat5a, Prrx2; phase 4 (4–6d; 7 transcription factors): Hod, Maf, Foxf2, Sox9, Stat1, Foxd1 and Neo1; phase 5 (8–14d; 24 transcription factors): Stat2, Esr1, Klf9, Klf13, AC162313.5, Cml3, Pou6f1, Pura, Nfat5, Zfp521, Trib3, Ddit3, 2210012G02Rik, Clock, Irf7, Nr3c1, Irf9, Zhx2, Sqstm1, Znfx1, Atf5, Hoxa9, Nr1d2 and Nfe2l1.
Found at: doi:10.1371/journal.pgen.1001019.s001 (1.10 MB TIF)

Figure S2 *Id4* expression pattern in ST2 osteoblast (A) and adipocyte (B) differentiation. Relative expression levels of *Id4* mRNA were measured by qRT-PCR.
Found at: doi:10.1371/journal.pgen.1001019.s002 (0.16 MB TIF)

Figure S3 4-week-old *Id4*$^{-/-}$ mice show decrease of growth plate in tibia. (A,B) Villanueva staining of growth plate of *Id4*$^{+/+}$ (A) and *Id4*$^{-/-}$ (B) mice tibia. The original magnifications and scale bars of the images are ×64 and 500 μm. (C) Growth plate width in tibia. (D) Longitudinal Growth Rate (Lo. G. R) in tibia. All data were subjected to Student's t-tests. ***p<0.005 versus control. Each error bar represents the mean±SE of *Id4*$^{+/+}$ (n = 6) and *Id4*$^{-/-}$ (n = 6), respectively.
Found at: doi:10.1371/journal.pgen.1001019.s003 (2.67 MB TIF)

Figure S4 Id4 associates with Hey2. (A) Isolation of bHLH transcription factors binding with Id4 was performed by immunoprecipitation (IP). IP was carried out using anti-FLAG antibody and Western blot analysis (WB) was performed using anti-HA antibody. Arrowheads indicate that Hey2 binds with Id4. (B) Direct interaction of recombinant glutathione S-transferase-tagged Id4 (GST-Id4) and recombinant FLAG-tagged Hey2 (FLAG-Hey2) was confirmed *in vitro*. The GST-pull down assay performed using glutathione sepharose beads bound to recombinant GST-Id4. Recombinant FLAG-Hey2 was detected with anti-FLAG antibody.
Found at: doi:10.1371/journal.pgen.1001019.s004 (0.22 MB TIF)

Figure S5 Expression level of osteoblast marker *in vivo*. (A) Ratio of relative *Bglap1* mRNA expression level between osteoblast-induced POB and non-induced POB from *Id4*$^{+/+}$ and *Id4*$^{-/-}$ neonatal calvarial bone. *Id4*$^{+/+}$ (n = 37), *Id4*$^{-/-}$ (n = 21). qRT-PCR data were subjected to Student's t-tests. **p<0.01 versus control. (B) Relative expression levels of *Id4* and *Bglap1* mRNA in *Id4*$^{+/+}$ and *Id4*$^{-/-}$ mouse embryo (E18.5) posterior limb were measured by qRT-PCR. *Id4*$^{+/+}$ (n = 1), *Id4*$^{-/-}$ (n = 4). Each error bar represents the mean±SE of triplicates.
Found at: doi:10.1371/journal.pgen.1001019.s005 (0.18 MB TIF)

Table S1 List of transcription factors expressed in induced ST2 cells differentiating into osteoblasts or adipocytes. Bhlh members are indicated using bold type. Arrows indicate up- (↑), down-regulated (↓), or up- and down-regulated (↑ ↓) transcription factors. No change in expression levels is symbolized by the almost equal sign (≈).
Found at: doi:10.1371/journal.pgen.1001019.s006 (0.10 MB XLS)

Acknowledgments

We greatly appreciate the technical assistance of M. Iseki, S. Okumura, M. Kitazato, M. Otsu, and K. Tanaka. We are grateful to K. Kano, M. Kohda, A. Itoh, H. Asahara, Y. Ito, and H. Iseki for their thoughtful discussion. We thank Y. Hayashizaki, J. Kawai, and H. Suzuki for critical suggestions and supporting the project.

Author Contributions

Conceived and designed the experiments: Y Tokuzawa, K Yagi, Y Mizuno, Y Okazaki. Performed the experiments: Y Tokuzawa, K Yagi, Y Yamashita, Y Ninomiya, Y Kanesaki-Yatsuka, M Akita, H Motegi, S Wakana, T Noda, Y Mizuno. Analyzed the data: Y Tokuzawa, Y Yamashita, Y Nakachi, I Nikaido, H Bono. Contributed reagents/materials/analysis tools: F Sablitzky, S Arai, R Kurokawa, T Fukuda, T Katagiri. Wrote the paper: Y Tokuzawa, K Yagi, Y Nakachi, C Schönbach, T Suda, Y Okazaki.

References

1. Burkhardt R, Kettner G, Bohm W, Schmidmeier M, Schlag R, et al. (1987) Changes in trabecular bone, hematopoiesis and bone marrow vessels in aplastic anemia, primary osteoporosis, and old age: a comparative histomorphometric study. Bone 8: 157–164.
2. Nuttall ME, Gimble JM (2004) Controlling the balance between osteoblastogenesis and adipogenesis and the consequent therapeutic implications. Curr Opin Pharmacol 4: 290–294.
3. Akune T, Ohba S, Kamekura S, Yamaguchi M, Chung UI, et al. (2004) PPARgamma insufficiency enhances osteogenesis through osteoblast formation from bone marrow progenitors. J Clin Invest 113: 846–855.
4. Kobayashi H, Gao Y, Ueta C, Yamaguchi A, Komori T (2000) Multilineage differentiation of Cbfa1-deficient calvarial cells in vitro. Biochem Biophys Res Commun 273: 630–636.
5. Lian JB, Stein GS, Javed A, van Wijnen AJ, Stein JL, et al. (2006) Networks and hubs for the transcriptional control of osteoblastogenesis. Rev Endocr Metab Disord 7: 1–16.
6. Nishimura R, Hata K, Ikeda F, Ichida F, Shimoyama A, et al. (2008) Signal transduction and transcriptional regulation during mesenchymal cell differentiation. J Bone Miner Metab 26: 203–212.
7. Takada I, Mihara M, Suzawa M, Ohtake F, Kobayashi S, et al. (2007) A histone lysine methyltransferase activated by non-canonical Wnt signalling suppresses PPAR-gamma transactivation. Nat Cell Biol 9: 1273–1285.
8. Iwata T, Kawamoto T, Sasabe E, Miyazaki K, Fujimoto K, et al. (2006) Effects of overexpression of basic helix-loop-helix transcription factor Dec1 on osteogenic and adipogenic differentiation of mesenchymal stem cells. Eur J Cell Biol 85: 423–431.
9. Buskin JN, Hauschka SD (1989) Identification of a myocyte nuclear factor that binds to the muscle-specific enhancer of the mouse muscle creatine kinase gene. Mol Cell Biol 9: 2627–2640.
10. Arnold HH, Braun T (1996) Targeted inactivation of myogenic factor genes reveals their role during mouse myogenesis: a review. Int J Dev Biol 40: 345–353.
11. Kim JB, Spiegelman BM (1996) ADD1/SREBP1 promotes adipocyte differentiation and gene expression linked to fatty acid metabolism. Genes Dev 10: 1096–1107.
12. Ross SE, Greenberg ME, Stiles CD (2003) Basic helix-loop-helix factors in cortical development. Neuron 39: 13–25.
13. Ross DA, Hannenhalli S, Tobias JW, Cooch N, Shiekhattar R, et al. (2006) Functional analysis of Hes-1 in preadipocytes. Mol Endocrinol 20: 698–705.
14. Lee JS, Thomas DM, Gutierrez G, Carty SA, Yanagawa S, et al. (2006) HES1 cooperates with pRb to activate RUNX2-dependent transcription. J Bone Miner Res 21: 921–933.
15. Tontonoz P, Hu E, Graves RA, Budavari AI, Spiegelman BM (1994) mPPAR gamma 2: tissue-specific regulator of an adipocyte enhancer. Genes Dev 8: 1224–1234.
16. Hu E, Liang P, Spiegelman BM (1996) AdipoQ is a novel adipose-specific gene dysregulated in obesity. J Biol Chem 271: 10697–10703.
17. Bedford L, Walker R, Kondo T, van Cruchten I, King ER, et al. (2005) Id4 is required for the correct timing of neural differentiation. Dev Biol 280: 386–395.
18. Sun XH, Copeland NG, Jenkins NA, Baltimore D (1991) Id proteins Id1 and Id2 selectively inhibit DNA binding by one class of helix-loop-helix proteins. Mol Cell Biol 11: 5603–5611.
19. Iso T, Sartorelli V, Poizat C, Iezzi S, Wu HY, et al. (2001) HERP, a novel heterodimer partner of HES/E(spl) in Notch signaling. Mol Cell Biol 21: 6080–6089.
20. Komori T, Yagi H, Nomura S, Yamaguchi A, Sasaki K, et al. (1997) Targeted disruption of Cbfa1 results in a complete lack of bone formation owing to maturational arrest of osteoblasts. Cell 89: 755–764.

21. Otto F, Thornell AP, Crompton T, Denzel A, Gilmour KC, et al. (1997) Cbfa1, a candidate gene for cleidocranial dysplasia syndrome, is essential for osteoblast differentiation and bone development. Cell 89: 765–771.
22. Nakashima K, Zhou X, Kunkel G, Zhang Z, Deng JM, et al. (2002) The novel zinc finger-containing transcription factor osterix is required for osteoblast differentiation and bone formation. Cell 108: 17–29.
23. Ducy P, Karsenty G (1995) Two distinct osteoblast-specific cis-acting elements control expression of a mouse osteocalcin gene. Mol Cell Biol 15: 1858–1869.
24. Suh JH, Lee HW, Lee JW, Kim JB (2008) Hes1 stimulates transcriptional activity of Runx2 by increasing protein stabilization during osteoblast differentiation. Biochem Biophys Res Commun 367: 97–102.
25. Kulterer B, Friedl G, Jandrositz A, Sanchez-Cabo F, Prokesch A, et al. (2007) Gene expression profiling of human mesenchymal stem cells derived from bone marrow during expansion and osteoblast differentiation. BMC Genomics 8: 70.
26. Liu T, Gao Y, Sakamoto K, Minamizaio T, Furukawa K, et al. (2007) BMP-2 promotes differentiation of osteoblasts and chondroblasts in Runx2-deficient cell lines. J Cell Physiol 211: 728–735.
27. Sciaudone M, Gazzerro E, Priest L, Delany AM, Canalis E (2003) Notch 1 impairs osteoblastic cell differentiation. Endocrinology 144: 5631–5639.
28. Nobta M, Tsukazaki T, Shibata Y, Xin C, Moriishi T, et al. (2005) Critical regulation of bone morphogenetic protein-induced osteoblastic differentiation by Delta1/Jagged1-activated Notch1 signaling. J Biol Chem 280: 15842–15848.
29. Maeda Y, Tsuji K, Nifuji A, Noda M (2004) Inhibitory helix-loop-helix transcription factors Id1/Id3 promote bone formation in vivo. J Cell Biochem 93: 337–344.
30. Katagiri T, Imada M, Yanai T, Suda T, Takahashi N, et al. (2002) Identification of a BMP-responsive element in Id1, the gene for inhibition of myogenesis. Genes Cells 7: 949–960.
31. Lopez-Rovira T, Chalaux E, Massague J, Rosa JL, Ventura F (2002) Direct binding of Smad1 and Smad4 to two distinct motifs mediates bone morphogenetic protein-specific transcriptional activation of Id1 gene. J Biol Chem 277: 3176–3185.
32. Zhang Y, Hassan MQ, Li ZY, Stein JL, Lian JB, et al. (2008) Intricate gene regulatory networks of helix-loop-helix (HLH) proteins support regulation of bone-tissue related genes during osteoblast differentiation. J Cell Biochem 105: 487–496.
33. Wan Y, Chong LW, Evans RM (2007) PPAR-gamma regulates osteoclastogenesis in mice. Nat Med 13: 1496–1503.
34. Mizuno Y, Yagi K, Tokuzawa Y, Kanesaki-Yatsuka Y, Suda T, et al. (2008) miR-125b inhibits osteoblastic differentiation by down-regulation of cell proliferation. Biochem Biophys Res Commun 368: 267–272.
35. Yang S, Takahashi N, Yamashita T, Sato N, Takahashi M, et al. (2005) Muramyl dipeptide enhances osteoclast formation induced by lipopolysaccharide, IL-1 alpha, and TNF-alpha through nucleotide-binding oligomerization domain 2-mediated signaling in osteoblasts. J Immunol 175: 1956–1964.
36. Yagi K, Kondo D, Okazaki Y, Kano K (2004) A novel preadipocyte cell line established from mouse adult mature adipocytes. Biochem Biophys Res Commun 321: 967–974.
37. Irizarry RA, Bolstad BM, Collin F, Cope LM, Hobbs B, et al. (2003) Summaries of Affymetrix GeneChip probe level data. Nucleic Acids Res 31: e15.
38. Wakabayashi K, Okamura M, Tsutsumi S, Nishikawa NS, Tanaka T, et al. (2009) The peroxisome proliferator-activated receptor gamma/retinoid X receptor alpha heterodimer targets the histone modification enzyme PR-Set7/Setd8 gene and regulates adipogenesis through a positive feedback loop. Mol Cell Biol 29: 3544–3555.

J Orthop Sci (2010) 15:804–809
DOI 10.1007/s00776-010-1542-5

JOURNAL OF
ORTHOPAEDIC SCIENCE

Original article

Deformity of the great toe in fibrodysplasia ossificans progressiva

Yasuharu Nakashima[1,2], Nobuhiko Haga[2], Hiroshi Kitoh[2], Junji Kamizono[2], Koji Tozawa[3], Takenobu Katagiri[2], Takafumi Susami[2], Jun-ichi Fukushi[1], and Yukihide Iwamoto[1]

[1] Department of Orthopaedic Surgery, Kyushu University, 1-3-3 Maidashi, Higashi-ku, Fukuoka 812-8582, Japan
[2] Research Committee on Fibrodysplasia Ossificans Progressiva
[3] Beppu Developmental Medicine and Rehabilitation Center, Beppu, Japan

Abstract

Background. As invasive medical procedures can induce permanent heterotopic ossification in fibrodysplasia ossificans progressiva (FOP), caution should be exercised in clinical practice. The present study was conducted to examine the characteristics of the great toe deformity in patients with FOP, which may lead to an early diagnosis of this condition.

Methods. The subjects consisted of 31 feet from 16 FOP patients (8 males, 8 females) with an average age of 17.3 years (range 1–47 years) at the time of this study. Gross and radiographic findings, including the hallux valgus angles (HVA), intermetatarsal angles (IMA), and the deformity of the proximal phalanx and metatarsal bone, were examined.

Results. Of the 31 feet, 29 (93.5%) showed several degrees of great toe deformity. A shortened great toe was the typical gross finding and was observed in 20 feet (64.5%). The mean HVA and IMA were 19.7° and 8.5°, respectively; and 22 (71.0%) feet satisfied the radiographic definition of hallux valgus (HVA ≥ 20° or IMA ≥ 10°). The proximal phalanx was consistently shortened but morphologically dissimilar from case to case. The metatarsal bone was also shortened and sharpened to the medial side, deviating the proximal phalanx laterally from the metatarsal axis. Fusion between the distal and proximal phalanx occurred with advancing age. Only two feet in one patient showed no obvious deformity of the great toe.

Conclusions. A shortened great toe and hallux valgus were frequently found in patients with FOP. Shortening and sharpening of the proximal phalanx and metatarsal bone consistently existed and contributed to the great toe deformity. These findings were thought to exist from birth and may be a key to an early diagnosis.

Introduction

Fibrodysplasia ossificans progressiva (FOP) is a rare disease, affecting one in every two million people.[1,2] Starting in childhood, it involves progressive ossification of skeletal muscles, tendons, and ligaments throughout the body, leading to decreased range of joint motion and deformity in the limbs and trunk.[3–6] In the terminal phase, respiratory function is impaired due to limited movement of the thorax, and trismus is caused by a limited range of motion in the temporomandibular joint.[2,7] The overall prognosis for this disease is considered poor. Although this condition is inherited in an autosomal dominant fashion, sporadic cases are common. In 2006, mutated genes of the activin A receptor (*ACVR1*), a bone morphogenetic protein type I receptor, were reported to be responsible for this disease.[8] The identical mutation of the *ACVR1* gene was also confirmed in Japanese patients with FOP.[9,10]

"Flare-ups" develop in patients with FOP that involve swelling accompanied by warmth and pain. They usually occur during childhood and are found mainly in the spine, frequently a result of minor trauma such as a fall.[11] These flare-ups persist for 2–3 months. Although the swelling itself diminishes, the injured sites may show development of heterotopic ossification within several months. This ossification then spreads throughout the body as flare-ups occur repeatedly, resulting in gradually decreasing range of joint motion. Because some medical procedures can induce ossification, caution should be exercised in clinical practice. These procedures include resection of heterotopic ossification, biopsy, and intramuscular injection.[12] Kitterman et al. reported that unnecessary biopsies were conducted in 67% of patients, and heterotopic ossification lesions were resected in 26%. In 49% of patients, flare-ups induced by these invasive medical procedures led to permanent loss of motion.[12]

An early diagnosis is essential to avoid symptom progression through unnecessary medical procedures and to allow the earliest possible initiation of treatment.[13,14] The definitive diagnosis is currently made by identifying mutations of the *ACVR1* gene, but it also requires clinical findings suggestive of FOP. Congenital malformation of the great toe is reported to be a typical finding in FOP and plays an important role in making an early diagnosis, considering that flare-ups are initiated during childhood.[13–16] This particular deformity was present in 95% of FOP cases studied by Kitterman et al. using a patient survey,[12] an incidence that was reportedly close to 100% in other publications.[13,14] After radiographically examining 15 patients with FOP, Harrison et al. noted a higher incidence of hallux valgus than is seen in healthy individuals.[15] As far as we know, there were no detailed reports on deformities of the great toe among Asian patients with FOP, and few reports fully describe the condition of the phalanges and metatarsal bones that constitute this deformity. The present study was conducted to examine the deformity of the great toe in patients with FOP both grossly and radiographically to clarify its incidence and to gather specific details regarding the affected bones.

Offprint requests to: Y. Nakashima
Received: July 6, 2010 / Accepted: August 5, 2010

Materials and methods

Subjects

The present study protocol was approved by our institutional review board. The subjects included 16 patients (32 feet) who were diagnosed with FOP at health care facilities where members of the Research Committee on Fibrodysplasia Ossificans Progressiva practiced. The details of the subjects are shown in Table 1. All the subjects were Japanese. There were eight males and eight females, with an average age of 17.3 years (range 1–47 years) at the time of this study. Patient 9 had had a corrective osteotomy of the left great toe when he was 7 years old. His left great toe was totally ankylosed from the metatarsal bone to the distal phalanx due to the surgical procedure, and his left toe therefore was excluded from this study. The remaining 31 feet in 16 subjects were included.

Gross findings of the great toe deformity

A shortened great toe and hallux valgus were the two major deformities evaluated (Figs. 1, 2). The tip of the great toe located proximal to the distal interphalangeal joint of the second toe was used as an indication of a shortened great toe in this study. Although the hallux valgus was defined by the radiographic measurement described below, gross findings were also described. In addition, the loss of the great toe itself or other toe was recorded.

Radiographic findings of the great toe

The hallux valgus angle (HVA) and the angle between the first and second metatarsal bones (IMA) were measured as indices of hallux valgus (Fig. 1). Hallux valgus was defined as present if the HVA was ≥20° and/or the IMA was ≥10°.[16] Because the deformity of the proximal phalanx and metatarsal bone varied among the feet, its shape and length were described. The presence or absence of fusion with the phalanges was also recorded and examined in relation to the patient's age.

Table 1. Patient demographics and morphology data

Case	Age (years)	Sex	Shortened great toe (right/left)	HVA (°) (right/left)	IMA (°) (right/left)	Fusion of proximal and distal phalanx (right/left)	Tapered distal metatarsal bone (right/left)
1	1	M	+/+	45/32	18/13	–/–	ND/ND
2	4	F	–/–	10/8	3/10	–/–	+/+
3	5	M	+/+	45/30	7/12	–/–	+/+
4	5	M	+/+	11/30	10/15	–/–	+/+
5	5	M	+/+	6/5	1/7	–/–	+/+
6	9	F	–/–	19/12	7/5	–/–	–/–
7	11	M	+/–	28/10	13/12	–/–	+/+
8	12	F	–/–	22/20	10/9	–/–	+/+
9	17	M	+/ND	25/ND	7/ND	–/ND	–/ND
10	17	F	–/–	25/14	6/9	+/+	+/+
11	22	M	+/+	20/6	10/0	+/+	+/+
12	24	F	–/–	10/13	8/7	+/+	+/+
13	27	F	+/+	28/22	11/2	+/+	+/+
14	34	M	+/+	20/7	10/2	+/+	+/–
15	37	F	+/+	30/25	10/10	+/+	+/–
16	47	F	+/+	20/15	10/10	+/+	+/–

HVA, hallux valgus angle; IMA, intermetatarsal angle; ND, not determined

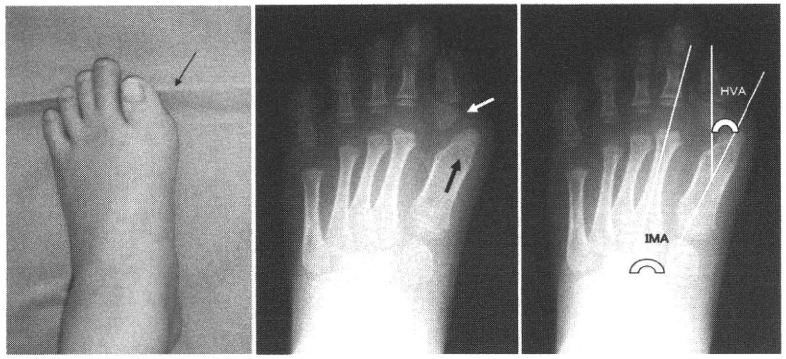

Fig. 1. Foot of a 5-year-old boy shows typical findings of fibrodysplasia ossificans progressiva (FOP). Note the shortened great toe (**a**, *arrow*) and the short and triangular proximal phalanx (**b**, *white arrow*). The metatarsal bone tapers at the distal end and deviates medially (*black arrow*). The proximal phalanx faces the lateral side of the distal metatarsal bone. **c** Hallux valgus angle (HVA) and the angle between the first and second metatarsal bones (IMA)

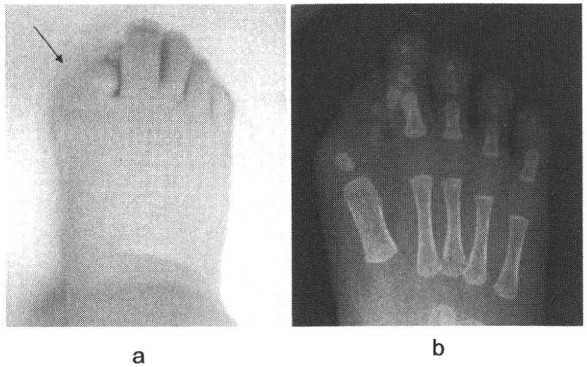

Fig. 2. **a** Note the shortened great toe with severe hallux valgus (*arrow*) in a 1-year-old boy. **b** The HVA and IMA are 45° and 18°, respectively. This case suggests the inherent deformity of the great toe in patients with FOP

Statistics

Patients were divided into two groups by the age at skeletal maturity (15 years old). Group 1 included individuals <15 years old (cases 1–8); and group 2 included those ≥15 years old (cases 9–16). The impact of age on the above-mentioned deformity of the great toe was examined by comparing these two groups using Fisher's exact test and the Mann-Whitney U-test. Significance was determined if $P < 0.05$.

Table 2. Comparison of the morphological data in groups 1 and 2

Parameter	Group 1: age <15 years (16 feet)	Group 2: age ≥15 years (15 feet)	*P*
Shortened great toe	56.3%	73.3%	0.4578
HVA[a]	20.8° ± 13.1°	18.7° ± 7.5°	0.8740
IMA[a]	9.5° ± 4.4°	7.5° ± 3.5°	0.1923
Fusion of proximal and distal phalanx	0	93.3%	<0.0001
Tapered distal metatarsal bone	75.0%	73.3%	0.6513

[a] Results are the mean ± SD

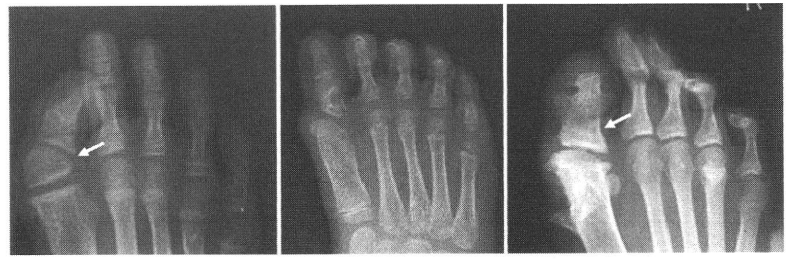

Fig. 3. Variations of the great toe deformity found in patients with FOP. **a** Triangular proximal phalanx and hallux valgus (*arrow*) in a 17-year-old boy. **b** Trapezoidal proximal phalanx and sharpened metatarsal bone without shortening or hallux valgus in a 4-year-old girl. **c** Fusion of the proximal and distal phalanx and a shortened great toe (*arrow*) in a 27-year-old woman

Results

Gross deformity of the great toe

A shortened great toe was observed in 22 of 33 feet (66.7%) (Table 1; Figs. 1, 2). Hallux valgus was observed along with the shortened great toes in most cases; five feet showed only great toe shortening. We did not detect loss of the great toe itself or of its nail in any of cases examined in this study, nor was there a loss of other toes.

Radiographic findings

The mean HVA was 19.7° (range 5°–45°). The mean IMA was 8.5° (range 2°–18°). Of the 31 feet, 22 (71.0%) exhibited hallux valgus with HVA > 20° or IMA > 10°. There were no significant differences in the HVA (20.8° vs. 18.7°) or the IMA (9.5° vs. 7.5°) between groups 1 and 2 ($P > 0.05$) (Table 2).

Deformity of the proximal phalanx was not uniform, with shapes that ranged from triangular to trapezoidal (Fig. 3). They were often short and small and were located lateral to the axis of the metatarsal bone. The first metatarsal bone was tapered at the distal end and shorter in length in 74.2% of the feet. The axis of the metatarsal bone was deviated medially, and the proximal phalanx faced the lateral side of the distal metatarsal bone, leading to the shortened great toe and hallux valgus deformity.

Fusion of the proximal and distal phalanx was observed in 14 feet (45.2%). Fusion was observed more frequently among older patients, occurring in 93.3% of feet in group 2. In contrast, no fusion was observed in the younger group ($P < 0.0001$) (Table 2).

In all, 29 feet (93.5%) in 15 patients showed several degrees of the deformities described above. Only two feet in one case (9-year-old girl) did not show any deformities at the time of this study (Fig. 4), although she showed the typical findings of FOP on her back and other joints (data not shown).

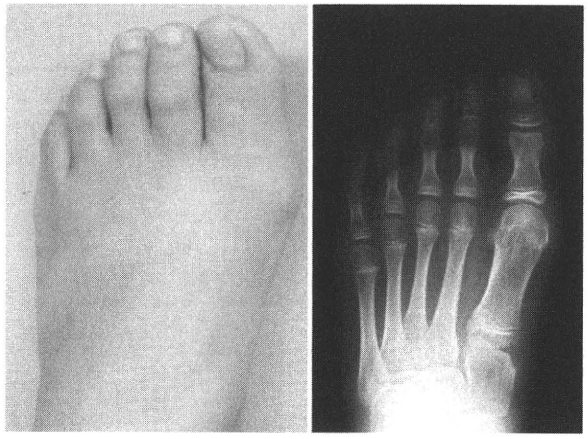

a b

Fig. 4. a, b A 9-year-old girl without the typical great toe deformity. Her foot does not show shortening or hallux valgus deformity

Discussion

In the present study, deformity of the great toe was grossly and radiographically examined in 16 Japanese patients with diagnosed FOP. In all 29 feet (93.5%) of 16 patients showed several degrees of great toe deformity. A shortened great toe was the typical gross finding and was observed in 64.5%; and 22 feet (71.0%) satisfied the radiographic definition of hallux valgus. The proximal phalanx was consistently shortened; and the metatarsal bone was sharpened to the medial side, deviating the proximal phalanx laterally. Fusion between the distal and proximal phalanx occurred with advancing age.

Because deformity of the great toe is known to be present at birth, it is important to diagnose FOP early. Kaplan et al. suggested that it is the most useful finding compared to other findings for an early diagnosis of FOP.[13] Kitterman et al. and other authors reported that deformity of the great toe was present in almost 100% of patients with FOP.[12,13] In the present study, deformities of the great toe, such as shortened length or valgus angulation, were present in 93% of cases. The presence of the deformity in a 1-year-old boy suggested the inherent condition of this deformity, and our results showed its high diagnostic value.

Deformity of the great toe comprises a deformity of the proximal phalanx and the metatarsal bone, as previously reported[15]; even so, there was a wide variation in the deformity of these bones found in the present study. The proximal phalanx was morphologically dissimilar from case to case; however, they were consistently shortened and were often located lateral to the axis of the metatarsal bones at its distal end. The metatarsal bone was also shortened and sharpened to the medial side, deviating the proximal phalanx laterally from the metatarsal axis. These deformities further exacerbated the shortening and valgus of the whole great toe.

According to Connor and Evans,[2] some deformities of the great toe often change with age. In fact, in our study, there was significant fusion of the proximal and distal phalanges in patients ≥15 years of age, whereas such a change was not common in patients <15 years in this study. Therefore, certain great toe deformities may still develop over time in the 9-year-old girl who was the only patient without apparent deformities in the present study.

Skeletal malformation in the extremities was not limited to the great toe but was also observed in thumbs from the early periods. Connor and Evans showed short thumbs due to short first metacarpals in 59% of patients and fifth-finger clinodactyly in 44%.[2] Smith et al. reported 13 patients with similar findings.[5] Among the available radiographs of three patients in our group I (younger group), all six thumbs were short without obvious angular deformity (data not shown). The first metacarpal bones were short, and the distal and proximal phalanges had an almost normal shape, as previously reported. Three fifth fingers showed several degrees of clinodactyly. As the deformity of the upper extremity is more likely to being found, the short thumbs coupled with the deformity of the great toe may contribute the early diagnosis of FOP.

The genetic mutation associated with FOP usually involves a change in the 206th amino acid of the *ACVR1* gene, which is commonly R to H, although other mutations have been reported. Furuya et al. reported a patient with FOP whose 356th amino acid, G, was replaced by D in the *ACVR1* gene. The great toe itself was missing on both feet of this patient, as were the thumbs.[17] Thus, among mutations of the *ACVR1* gene, phenotypes can differ depending on the site of mutation. In the present study, the only patient (9-year-old girl) without deformity of the great toe had the common mutation of *ACVR1* (R206H). Further accumulation of cases is necessary to clarify the relation between these genetic mutations and phenotypes.

The primary limitation of the present study is that it was conducted as a cross-sectional study. Because the patients were not observed over time, the impact of age could only be speculated. Our findings indicated that the incidence of fusion of the proximal and distal phalanges increased with age. We therefore predict that fusion would also become more common over time in group 1. It is necessary to follow patients with serial examinations.

Conclusion

Shortening and valgus deformities of the great toe were present in most of the patients studied. The misshaped great toe consisted of a deformity of the proximal phalanx, its fusion with the distal phalanx, and deformity of the metatarsal bone. Deformity of the great toe is thought to be present at birth in patients with FOP and therefore is an important finding for an early diagnosis.

Acknowledgment. This work was supported by the project "Research on Measures for Intractable Diseases," sponsored by the Ministry of Health, Labor, and Welfare of Japan.

The authors thank Dr. Masanori Fujii for his help in preparing this manuscript.

References

1. Delatycki M, Rogers JG. The genetics of fibrodysplasia ossificans progressiva. Clin Orthop 1998;346:15–8.
2. Connor JM, Evans DA. Fibrodysplasia ossificans progressiva: the clinical features and natural history of 34 patients. J Bone Joint Surg Br 1982;64:76–83.
3. Rogers JG, Geho WB. Fibrodysplasia ossificans progressiva: a survey of forty-two cases. J Bone Joint Surg Am 1979;61: 909–14.
4. Cohen RB, Hahn GV, Tabas JA, Peeper J, Levitz CL, Sando A, et al. The natural history of heterotopic ossification in patients who have fibrodysplasia ossificans progressiva: a study of forty-four patients. J Bone Joint Surg Am 1993;75:215–9.
5. Smith R, Athanasou NA, Vipond SE. Fibrodysplasia (myositis) ossificans progressiva: clinicopathological features and natural history. Q J Med 1996;89:445–6.
6. Smith R. Fibrodysplasia (myositis) ossificans progressiva: clinical lessons from a rare disease. Clin Orthop 1998;346:7–14.
7. Vashisht R, Prosser D. Anesthesia in a child with fibrodysplasia ossificans progressiva. Paediatr Anaesth 2006;16:684–8.
8. Shore EM, Xu M, Feldman GJ, Fenstermacher DA, Cho TJ, Choi IH, et al. A recurrent mutation in the BMP type I receptor ACVR1 causes inherited and sporadic fibrodysplasia ossificans progressiva. Nat Genet 2006;38:525–7.
9. Nakajima M, Haga N, Takikawa K, Manabe N, Nishimura G, Ikegawa S. The ACVR1 617G > A mutation is also recurrent in three Japanese patients with fibrodysplasia ossificans progressiva. J Hum Genet 2007;52:473–5.
10. Fukuda T, Kohda M, Kanomata K, Nojima J, Nakamura A, Kamizono J, et al. Constitutively activated ALK2 and increased SMAD1/5 cooperatively induce bone morphogenetic protein signaling in fibrodysplasia ossificans progressiva. J Biol Chem 2009;284:7149–56.
11. Glaser DL, Rocke DM, Kaplan FS. Catastrophic falls in patients who have fibrodysplasia ossificans progressiva. Clin Orthop 1998;346:110–6.
12. Kitterman JA, Kantanie S, Rocke DM, Kaplan FS. Iatrogenic harm caused by diagnostic errors in fibrodysplasia ossificans progressiva. Pediatrics 2005;116:654–61.
13. Kaplan FS, Xu M, Glaser DL, Collins F, Connor M, Kitterman J, et al. Early diagnosis of fibrodysplasia ossificans progressiva. Pediatrics 2008;121:1295–300.
14. Kaplan FS, Le Merrer M, Glaser DL, Pignolo RJ, Goldsby RE, Kitterman JA, et al. Fibrodysplasia ossificans progressiva. Best Pract Res Clin Rheumatol 2008;22:191–205.
15. Harrison RJ, Pitcher JD, Mizel MS, Temple HT, Scully SP. The radiographic morphology of foot deformities in patients with fibrodysplasia ossificans progressiva. Foot Ankle Int 2005;26: 937–41.
16. Coughlin MJ, Jones CP. Hallux valgus: demographics, etiology, and radiographic assessment. Foot Ankle Int 2007;28:759–77.
17. Furuya H, Ikezoe K, Wang L, Ohyagi Y, Motomura K, Fujii N, et al. A unique case of fibrodysplasia ossificans progressiva with an ACVR1 mutation, G356D, other than the common mutation (R206H). Am J Med Genet A 2008;146A:459–63.

Cell Death and Differentiation (2010), 1–13

www.nature.com/cdd

BMP signalling permits population expansion by preventing premature myogenic differentiation in muscle satellite cells

Y Ono[1], F Calbaheu[1], JE Morgan[2], T Katagiri[3], H Amthor[4] and PS Zammit*[,1]

Satellite cells are the resident stem cells of adult skeletal muscle, supplying myonuclei for homoeostasis, hypertrophy and repair. In this study, we have examined the role of bone morphogenetic protein (BMP) signalling in regulating satellite cell function. Activated satellite cells expressed BMP receptor type 1A (BMPR-1A/Alk-3) and contained phosphorylated Smad proteins, indicating that BMP signalling is operating during proliferation. Indeed, exogenous BMP4 stimulated satellite cell division and inhibited myogenic differentiation. Conversely, interfering with the interactions between BMPs and their receptors by the addition of either the BMP antagonist Noggin or soluble BMPR-1A fragments, induced precocious differentiation. Similarly, blockade of BMP signalling by siRNA-mediated knockdown of BMPR-1A, disruption of the intracellular pathway by either Smad5 or Smad4 knockdown or inhibition of Smad1/5/8 phosphorylation with Dorsomorphin, also caused premature myogenic differentiation. BMP signalling acted to inhibit the upregulation of genes associated with differentiation, in part, through regulating Id1. As satellite cells differentiated, Noggin levels increased to antagonise BMP signalling, since Noggin knockdown enhanced proliferation and impeded myoblast fusion into large multinucleated myotubes. Finally, interference of normal BMP signalling after muscle damage *in vivo* perturbed the regenerative process, and resulted in smaller regenerated myofibres. In conclusion, BMP signalling operates during routine satellite cell function to help coordinate the balance between proliferation and differentiation, before Noggin is activated to antagonise BMPs and facilitate terminal differentiation.
Cell Death and Differentiation advance online publication, 6 August 2010; doi:10.1038/cdd.2010.95

Muscle satellite cells are the resident stem cells of skeletal muscle and supply myonuclei for postnatal muscle growth, and for maintenance and repair in adult.[1] Satellite cells are located on the surface of myofibres and are mitotically quiescent in healthy adult muscle. In response to cues for routine myofibre homoeostasis or hypertrophy, or the sporadic demands of muscle repair, satellite cells are activated to generate myoblasts that proliferate and eventually undergo myogenic differentiation to provide new myonuclei. Satellite cells also self-renew, thus maintaining a population of quiescent, undifferentiated precursors available to respond to repeated demand.[2–4]

Satellite cell function is controlled by various regulatory pathways, chief amongst them being Notch/Delta and Wnt signalling.[1] Many of these same regulatory networks also control embryonic myogenesis, in addition to many other processes, both during development and repair in adult. Another important network for organising embryonic and foetal myogenesis involves the Bone morphogenetic proteins (BMPs). BMPs belong to the transforming growth factor-β family and initiate signalling by binding to the transmembrane type 1 and type 2 BMP receptors (BMPRs). On BMP binding, type 1 and 2 receptors complex on the cell surface, allowing the constitutively active kinase of the type 2 receptor to transphosphorylate the type 1 receptor.[5] This in turn phosphorylates the R-Smads – Smad1, Smad5 and Smad8 (pSmad1/5/8) – which translocate to the nucleus to regulate transcription of target genes including *Ids*.[6–8] Inhibitor of differentiation/DNA-binding (Id) proteins (comprising Id1, 2, 3, 4) bind ubiquitously expressed E-proteins to form inactive heterodimers, thereby preventing the same E-proteins from binding with tissue-specific transcription factors such as MyoD and myogenin, a step necessary for their efficient function.[9] BMP signalling can be modified in a number of ways, including through secreted antagonists such as Noggin, which bind BMPs with high affinity to interfere with interactions between BMPs and their receptors.[5]

Although crucial for bone and cartilage formation and repair,[5,10] BMPs also inhibit myogenic differentiation to prevent ectopic myogenesis in the lateral plate mesoderm.

[1]King's College London, Randall Division of Cell and Molecular Biophysics, New Hunt's House, Guy's Campus, London SE1 1UL, UK; [2]Dubowitz Neuromuscular Centre, UCL Institute of Child Health, 30 Guilford Street, London WC1N 1EH, UK; [3]Division of Pathophysiology, Research Centre for Genomic Medicine, Saitama Medical University, 1397-1 Yamane, Hidaka-shi, Saitama 350-1241, Japan and [4]UPMC INSERM, UMR S 974/CNRS UMR 7215, Institut de Myologie, 105 bd de l'Hôpital, 75013 Paris, France

*Corresponding author: PS Zammit, King's College London, Randall Division of Cell and Molecular Biophysics, New Hunt's House, Guy's Campus, London SE1 1UL, UK. Fax: +44 207 848 6435; E-mail: peter.zammit@kcl.ac.uk

Keywords: satellite cell; BMP; Noggin; Smad; Id1; skeletal muscle

Abbreviations: BMP, bone morphogenetic protein; BMPR-1A, bone morphogenetic protein receptor type 1A/Alk-3; sBMPR-1Af, soluble bone morphogenetic protein receptor 1A fragments; caBMPR-1A, constitutively active bone morphogenetic protein receptor type 1A; pSmad1/5/8, phosphorylated Smad1, Smad5 and Smad8; Id, inhibitor of differentiation/DNA-binding protein; FOP, Fibrodysplasia ossificans progressiva; EDL, extensor digitorum longus; MyHC, myosin heavy chain; CKM, Muscle creatine kinase; DAPI, 4,6-diamidino-2-phenylindole; T0, freshly isolated; T48, cultured for 48 h; T72, cultured for 72 h

Received 17.12.09; revised 14.6.10; accepted 15.6.10; Edited by R De Maria

In the dermomyotome, however, BMP signalling itself must be inhibited, to permit the onset of myogenesis.[11–14] BMPs not only impede myogenic differentiation in immortalised myogenic cell lines (e.g., C2) and primary myogenic cells *in vitro* but also induce osteoblastic gene expression and differentiation towards the osteoblast lineage.[15–18] Interestingly, although able to express early markers of osteogenic differentiation such as alkaline phosphatase, many primary myogenic cells also retain expression of proteins associated with myogenesis (e.g., Pax7 and MyoD) after exposure to BMPs for several days.[15,17] As intramuscular injection of certain BMPs (e.g., BMP2 and BMP4) can lead to ectopic bone formation *in vivo*,[19,20] these *in vitro* observations were thought to provide mechanistic insight into Fibrodysplasia ossificans progressiva (FOP), a rare disorder of skeletal malformations and progressive extra-skeletal ossification in muscle. FOP is caused by a mutation in *ALK-2*, which renders this BMPR type 1 (BMPR-1) constitutively active,[19] and inhibition of this mutant ALK-2 reduces ossification.[21] However, Lounev *et al.*[20] have recently shown that few (<5%) muscle progenitors actually contribute to BMP-induced heterotopic ossification *in vivo*.

In this study, we investigated the role of BMP signalling in satellite cell function during adult myogenesis. During activation and proliferation, satellite cells robustly express BMPR-1A (Alk-3), with pSmad1/5/8 and Smad4 present in their nuclei, indicative of operational BMP signalling. Exogenous BMP4 can sustain satellite cell division and reduce differentiation, with BMP4 functioning through BMPR-1A. Conversely, antagonising the interaction of BMP with its receptors or perturbing intracellular BMP signalling by either inhibiting Smad1/5/8 phosphorylation or reducing Smad5 or Smad4 levels, all induced premature differentiation. Manipulation of BMP signalling affected Id1 levels: a known inhibitor of differentiation that regulates the function of the myogenic regulatory factors (that comprise of Myf5, MyoD, myogenin and MRF4) through sequestration of E-proteins. Satellite cell progeny then upregulate the BMP antagonist Noggin as they differentiate, and knockdown of Noggin enhanced proliferation and impeded differentiation. As blockade of BMP signalling after muscle injury hindered regeneration, our observations show that BMP signalling is a potent regulator of routine satellite cell function in adult.

Results

BMP pathway proteins are present in activated and proliferating satellite cells. Satellite cell function can be modelled *in vitro*. On stimulation by mitogen-rich medium (termed plating or proliferation medium here), isolated Pax7-expressing quiescent satellite cells are activated and upregulate MyoD. Satellite cells then proliferate, before either downregulating Pax7, maintaining MyoD, inducing myogenin and proceeding to differentiate, or downregulating MyoD and maintaining Pax7, to return to a quiescent-like state, modelling self-renewal.[2,3]

To first determine the expression profile of BMPR-1A, we immunostained satellite cells retained in their niche on myofibres isolated from the extensor digitorum longus (EDL) muscle. BMPR-1A was undetectable in the vast majority of quiescent satellite cells on freshly isolated (T0) myofibres (Figure 1a). However, after culturing in plating medium for 48 (T48) or 72 h (T72), BMPR-1A became robustly expressed in activated and proliferating satellite cells (Figure 1a). *BMPR-1B* was not detectable by Q-PCR (data not shown), consistent with its absence in C2C12 myoblasts.[22] Intracellular BMP signalling through BMPR-1A operates by phosphorylation of the carboxyl terminal of R-Smad proteins. Immunostaining for either pSmad1/5/8 or Smad5, revealed a strong nuclear signal in activated and proliferating (T48 and T72), but not quiescent (T0), satellite cells (Figure 1b and c). The common-mediator Smad (Co-Smad) Smad4, which facilitates translocation of Smad1/5/8 to the nucleus and promotes their transcriptional activity,[5] was also present in the nuclei of activated satellite cells (Figure 1c). Thus, the expression dynamics of BMPR-1A, pSmad1/5/8, Smad4 and Smad5 mirror each other, and indicate that BMP signalling is operating in activated and proliferating satellite cells.

As Noggin-mediated BMP antagonism contributes to initiation of the myogenic programme during embryogenesis,[13] we hypothesised that Noggin may also modify BMP signalling in satellite cells. Noggin was undetectable in quiescent (T0), and at low levels in activated Pax7$^+$, satellite cells (Figure 2a and b). In contrast, Noggin was highly expressed by differentiating myoblasts at T72, as shown by co-immunostaining for Noggin and myogenin (Figure 2b). Culturing satellite cells attached to a myofibre provides a useful model for studying satellite cell activation, proliferation and the initial stages of differentiation. Later events, such as myoblast fusion into large multi-nucleated myotubes, however, are better studied in satellite cells isolated from their associated myofibre and plated onto Matrigel-coated culture dishes. Such plated satellite cell-derived myoblasts cultured in differentiation medium for 2 days clearly exhibited high Noggin levels in myotubes and other Pax7$^-$ cells (Figure 2c and d).

BMP regulates the balance between proliferation and differentiation in satellite cells. We next examined the effects of stimulating BMP signalling, and used administration of recombinant BMP4 to achieve this, as it is present in serum.[23] Addition of recombinant BMP4 protein (100 ng/ml) to EDL satellite cells retained in their niche on the myofibre significantly increased the number of Pax7$^+$MyoD$^+$ satellite cells, but decreased the number of cells with the differentiating Pax7$^-$MyoD$^+$ phenotype (Figure 3a). Inhibition of differentiation by BMP4 was confirmed by co-immunostaining for myogenin and Pax7 (Figure 3b). Plating medium contains chick embryo extract and horse serum, hence is rich in growth factors, and also contains BMP4.[23] Under these culture conditions, satellite cell proliferation is likely to be near maximal; hence, addition of BMP4 did not further increase cell division (Figure 3a and b). As satellite cells retained expression of genes associated with myogenesis, these short exposures to BMP4 did not induce any obvious loss of myogenic identity.

To interfere with BMP binding to its receptors, we added recombinant Noggin protein (50 ng/ml) or soluble BMPR-1A fragments (sBMPR-1Af; 200 ng/ml) to cultures of satellite cells associated with a myofibre for 72 h. Exposure to either Noggin

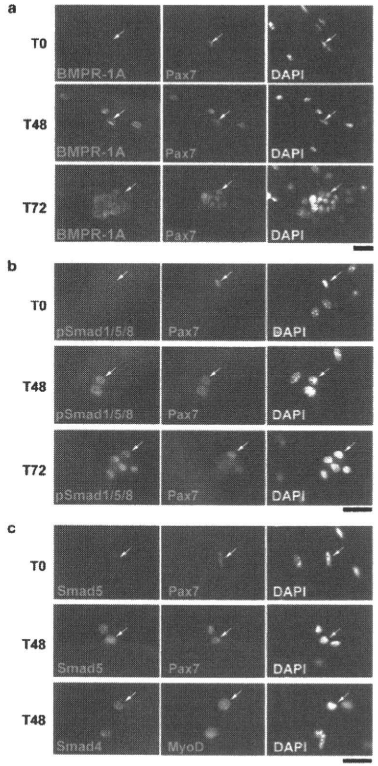

Figure 1 BMPR-1A, pSmad 1/5/8, Smad4 and Smad 5 are upregulated during satellite cell activation. Isolated EDL myofibres with their associated satellite cells were either immediately fixed (T0) or cultured in plating medium for either 48 h (T48) or 72 h (T72) before fixation and immunostaining. (**a**) BMPR-1A was undetectable on the majority of Pax7$^+$ quiescent cells at T0, but robustly expressed in both Pax7$^+$ and Pax7$^-$ cells at both T48 and T72. (**b**) Quiescent Pax7$^+$ satellite cells (T0) did not contain pSmad1/5/8, whereas pSmad1/5/8 became readily detectable in the nuclei of proliferating Pax7$^+$ cells at T48, and both Pax7$^+$ and Pax7$^-$ cells at T72. (**c**) In accordance with the dynamics of pSmad1/5/8 expression, Smad5 levels were very low/absent in quiescent satellite cells at T0, but upregulated in both proliferating Pax7$^+$ and MyoD$^+$ cells at T48, as was Smad4. Arrows indicate the same satellite cell at each time point to aid comparison. Representative images from at least three independent experiments are shown. Scale bar equals 30 μm

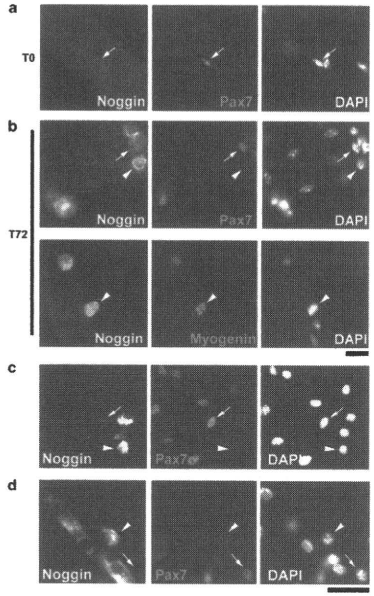

Figure 2 Noggin is highly expressed in satellite cell progeny committing to myogenic differentiation. Isolated EDL myofibres with their associated satellite cells were either immediately fixed (T0) or cultured in plating medium for 72 h (T72) before fixation and immunostaining. (**a**) Noggin was not expressed in quiescent Pax7$^+$ satellite cells (arrows) at T0. (**b**) After culture, Noggin was highly expressed in both Pax7$^-$ and Myogenin$^+$ cells committed to myogenic differentiation (arrowheads) at T72, but at much lower levels in Pax7$^+$ cells (arrows). (**c** and **d**) Plated satellite cell-derived myoblasts were cultured in differentiation medium for 2 days and immunostained for Noggin and Pax7. (**c**) Pax7$^-$ differentiating cells (arrowheads) and (**d**) myotubes both expressed high levels of Noggin protein, while Noggin levels in Pax7$^+$ cells were low (arrows). Representative images from at least three independent experiments are shown. Scale bar equals 30 μm

or sBMPR-1Af resulted in a significant reduction in the mean total satellite cell number per myofibre, particularly of cells with the Pax7$^+$MyoD$^+$ phenotype (Figure 3a). Numbers of differentiating Pax7$^-$MyoD$^+$ cells were already increased at T48, and became the predominant phenotype at T72, signifying a precocious onset of differentiation (Figure 3a). There were also significantly fewer self-renewing Pax7$^+$MyoD$^-$ cells present at T72 (Figure 3a). Co-immunostaining for Pax7 and myogenin confirmed that both Noggin and sBMPR-1Af enhanced differentiation, revealing a significant increase in cells with the Pax7$^-$myogenin$^+$

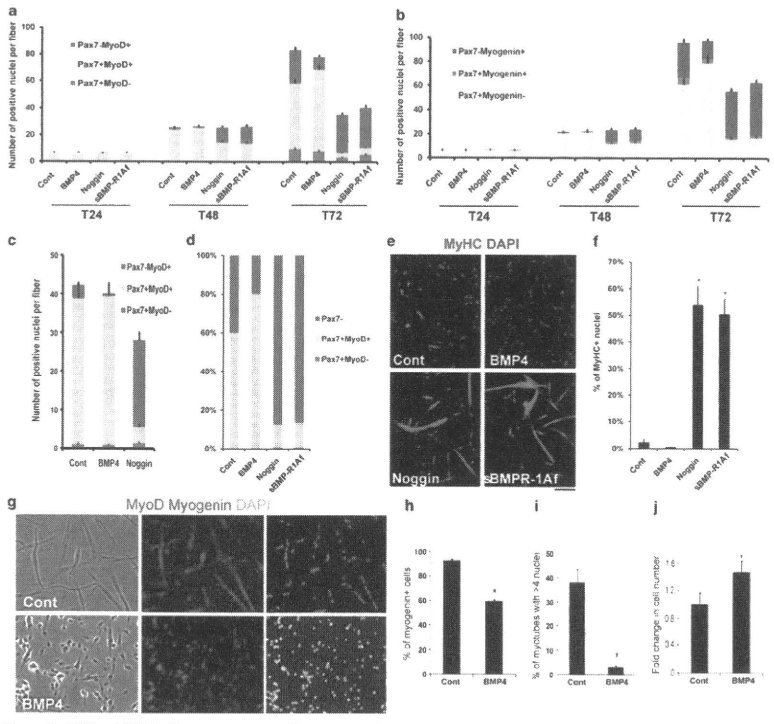

Figure 3 Inhibition of BMP signalling promotes myogenic differentiation in satellite cells. Isolated myofibres associated with satellite cells, or plated satellite cell-derived myoblasts, were cultured in the presence of recombinant BMP4 protein (100 ng/ml), recombinant Noggin protein (50 ng/ml) or sBMPR-1Af (200 ng/ml). (**a**) EDL myofibres were cultured in plating medium supplemented with BMP4, Noggin or sBMPR-1Af, then fixed after 24 (T24), 48 (T48) or 72 (T72) h and immunostained for Pax7 and MyoD. BMP4 reduced the number of Pax7$^-$MyoD$^+$ cells. Both Noggin and sBMPR-1Af reduced the mean total number of cells per myofibre and promoted myogenic differentiation (increase of the Pax7$^-$MyoD$^+$ phenotype). (**b**) Co-immunostaining isolated myofibres for Pax7, and myogenin confirmed that BMP4 inhibited myogenic differentiation, whereas Noggin and sBMPR-1Af promoted it, as shown by the increase of satellite cell progeny with the Pax7$^-$myogenin$^+$ phenotype. (**c**) Treatment of masseter-derived satellite cells with BMP4 or Noggin for 72 h produced the same result as for EDL cells, that is, BMP4 inhibited, whereas Noggin induced, myogenic differentiation. (**d**–**f**) To examine the effects of these recombinant proteins on the later stages of myogenesis, EDL satellite cells were plated and cultured in the presence of recombinant BMP4, Noggin or sBMPR-1Af in plating medium for 4 days (with the medium changed every other day). (**d**) Co-immunostaining for Pax7 and MyoD again showed a dramatic increase in the proportion of cells with the differentiating Pax7$^-$ phenotype when exposed to either Noggin or sBMPR-1Af. (**e**, quantified in **f**) Immunostaining for MyHC revealed that exposure to either Noggin or sBMPR-1Af resulted in precocious differentiation and formation of large multi-nucleated myotubes. (**g**–**j**) To better examine the effects of BMP on satellite cell proliferation and myogenic progression, plated satellite cells were also cultured in differentiation medium supplemented with recombinant BMP4 protein (200 ng/ml) and immunostained for MyoD and myogenin (**g**, quantified in **h**–**j**). Exposure to BMP4 significantly reduced the proportion of cells expressing myogenin (**h**) and fusing into large myotubes (**i**), but stimulated continued cell proliferation, resulting in a 1.46 ± 0.2-fold increase in total cell number (**j**). Data are mean ± S.E.M. (**a**–**c**) or mean ± S.D. (**f**–**j**) from at least three independent experiments. Asterisk indicates that data are significantly different from controls ($P<0.05$) using Student's *t*-test. Scale bar equals 100 μm for **e**

phenotype (Figure 3b). These effects were not restricted to satellite cells from somite-derived muscles, as those from the branchiomeric masseter muscle, which has a different embryonic origin,[24] also exhibited fewer differentiating Pax7$^-$MyoD$^+$ cells in the presence of BMP4, but increased differentiation when exposed to Noggin (Figure 3c).

Culture in proliferation medium does not readily support differentiation of plated satellite cells. Addition of recombinant BMP4 resulted in a higher proportion of cells co-immunostained for Pax7 and MyoD (Figure 3d). The differentiation index under these culture conditions, however, is already so low that any inhibitory effect of BMP4 on formation of myosin heavy chain (MyHC) containing myocytes was not significant (Figure 3e, quantified in f). Addition of either Noggin or sBMPR-1Af, however, triggered a robust differentiation, as shown by both the reduced proportion of plated cells with Pax7 (Figure 3d) and the marked increase in myotubes containing MyHC (Figure 3e and f). The proportion of satellite cell progeny with the self-renewing $Pax7^+MyoD^-$ phenotype was also significantly increased, from effectively zero in control cultures to ~0.7% after exposure to either Noggin or sBMPR-1Af (Figure 3d).

Finally, we determined the effects of exogenous BMP4 on satellite cells after serum deprivation, which normally promotes myogenin expression, cell cycle exit and fusion into myotubes. However, addition of recombinant BMP4 (200 ng/ml) to differentiation medium led to a significant drop in the proportion of cells containing myogenin (Figure 3g, quantified in h) and fusing into myotubes (Figure 3g, quantified in i). On the other hand, MyoD remained readily detectable in the nuclei of these cells after exposure to BMP4 for 2 days (Figure 3g). Importantly, BMP4 caused a 1.46 ± 0.2-fold increase in total cell number, indicating that BMP4 not only inhibits differentiation but also stimulates satellite cell proliferation, despite serum depletion (Figure 3j).

BMP operates through BMPR-1A to prevent precocious differentiation. To determine whether BMP signalling was transduced through BMPR-1A in activated satellite cells, we used siRNA-mediated knockdown,[25] which reduced the mean total number of satellite cells per myofibre when assayed at T72 (Figure 4a, quantified in b). In particular, BMPR-1A knockdown significantly decreased the number of both $Pax7^+MyoD^+$ cells and $Pax7^+MyoD^-$ self-renewed cells, but not the number of $Pax7^-MyoD^+$ differentiating cells, which became the predominant phenotype (Figure 4b).

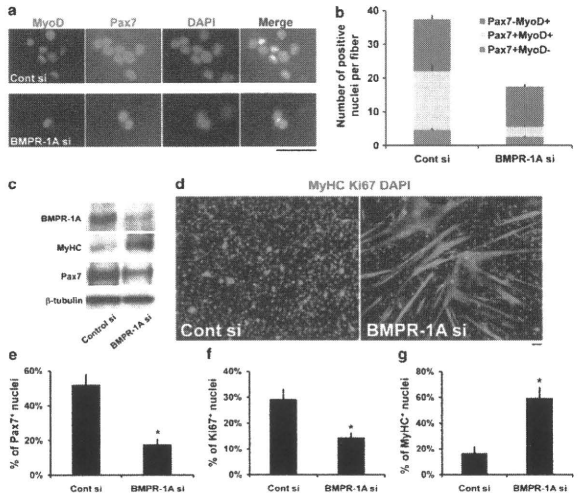

Figure 4 BMP signalling functions through BMPR-1A. We used siRNA-mediated protein knockdown to explore whether BMP signalling operates through BMPR-1A. (**a**, quantified in **b**) Control (Cont si) or BMPR-1A (BMPR-1Asi) siRNA were transfected into satellite cells retained in their niche on isolated EDL myofibers and cultured for ~2.5 days before fixation and co-immunostaining for Pax7 and MyoD. BMPR-1A knockdown reduced the mean total number of cells, especially the number of $Pax7^+MyoD^+$ cells. (**c–g**) Control siRNA or BMPR-1A siRNA duplexes were also transfected into plated satellite cell-derived myoblasts. (**c**) Immunoblot analysis clearly demonstrated efficient knockdown of BMPR-1A protein levels, which resulted in an upregulation of MyHC, but a downregulation of Pax7 (β-tubulin served as a protein loading control). (**d**, quantified in **e–g**) The effects of BMPR-1A knockdown were also examined by immunostaining for Pax7, Ki67 or MyHC in plated satellite cell-derived myoblasts cultured in proliferation medium for 3 days after transfection. (**d**) Representative images of Ki67 and MyHC immunostaining show that BMPR-1A knockdown inhibited cell proliferation and promoted myogenic differentiation. (**e and f**) There was a significant decrease in the proportion of cells containing Pax7 or Ki67 (proliferating) after BMPR-1A siRNA-transfection. (**g**) In contrast, there was a significant increase in the proportion of $MyHC^+$ differentiated cells and myotubes. Data are either mean ± S.E.M. (**b**) or mean ± S.D. (**e–g**) from at least three independent experiments. Asterisk denotes that data are significantly different from control ($P<0.05$). Scale bar equals 50 μm

The efficient reduction in BMPR-1A levels by siRNA was confirmed by western blot analysis of plated satellite cells, which also revealed decreased Pax7 levels, but an increase in the amount of MyHC (Figure 4c). Immunostaining (Figure 4d, quantified in e–g) confirmed that reducing BMPR-1A led to a reduction in the proportion of $Pax7^+$ cells (Figure 4e), which was accompanied by a significant reduction in $Ki67^+$ proliferating cells (Figure 4d and f). In contrast, there was an increase in the proportion of $MyHC^+$ differentiated cells after BMPR-1A knockdown (Figure 4d and g).

Blockade of intracellular BMP signalling promotes myogenic differentiation. We next analysed the pSmad1/5/8 signalling cascade.[5] The protein kinase inhibitor Dorsomorphin is a specific inhibitor of Smad1/5/8 phosphorylation by BMPRs.[26] Dorsomorphin (1–5 μM) was not toxic to plated satellite cells, as shown using the Tunel assay (data not shown). Exposure of cultured myofibres to Dorsomorphin significantly decreased the mean number of associated $Pax7^+MyoD^+$ satellite cells, and hence $Pax7^-MyoD^+$ differentiating cells became the main phenotype (Figure 5a). Dorsomorphin also induced myogenic differentiation in a dose-dependent (0.1–1.0 μM) manner in plated satellite cells maintained in proliferation medium (Figure 5b). Additionally, we also targeted Smad signalling using siRNA-mediated knockdown of Smad5 or Smad4, which effectively reduced the levels of the translated protein (Figure 5c and d). Co-immunostaining for Ki67 and MyHC revealed that Smad5 or Smad4 knockdown significantly reduced cell proliferation and induced precocious differentiation (Figure 5e, quantified in f and g).

BMP signalling regulates the ability of MyoD to activate its transcriptional targets. To understand how interference with BMP signalling promotes myogenic differentiation, we investigated Id1, a downstream target of BMPs[6–8] and a negative controller of MyoD and myogenin.[9,27] We recently showed that Id1 is highly expressed in proliferating satellite cells, before being downregulated during myogenic differentiation.[25] Immunostaining showed that exposure to Dorsomorphin to inhibit Smad1/5/8 phosphorylation reduced Id1 levels in both satellite cells retained in their niche on the myofibre (Figure 6a) and in plated satellite cells (Figure 6b).

Muscle creatine kinase (*CKM*) is a well-characterised gene and provides a useful tool to quantify both the ability of MyoD to transactivate its target genes, and myogenic differentiation.[27] Therefore, we measured the activity of a *CKM-luciferase* construct (*CKM-LUCpCS2*) in response to both exogenous Id1 and perturbation of BMP signalling (Figure 6c). As expected, *CKM-LUCpCS2* activity was significantly decreased after transfection with *Id1* (Figure 6c). Importantly, transfection of a plasmid encoding a constitutively active BMPR-1A (caBMPR-1A) that phosphorylates Smad1/5/8 in the absence of BMP ligands[28] also significantly reduced *CKM-LUCpCS2* activity (Figure 6c). In contrast, inhibition of Smad1/5/8 phosphorylation with Dorsomorphin significantly increased the activity of *CKM-LUCpCS2*, but Id1 was able to completely reverse this Dorsomorphin-mediated increase (Figure 6c). Finally, caBMPR-1A also reduced *CKM-LUCpCS2* activity back to control levels, despite the presence of Dorsomorphin (Figure 6c). Thus, BMP signalling in satellite cells acts to limit the transcriptional activation of genes controlled by MyoD and enhanced during differentiation.

Noggin antagonises BMPs to facilitate myogenic differentiation. Noggin is upregulated as satellite cells differentiate (Figure 2). To examine the role of Noggin, we first performed siRNA-mediated knockdown in plated satellite cells, and immunostaining showed that it worked efficiently (Figure 7a). Plated satellite cells transfected with Noggin siRNA and co-immunostained for Ki67 and MyHC (Figure 7b, quantified c–e) had a significantly increased proportion of proliferating $Ki67^+$ satellite cells (Figure 7c). However, the proportion of differentiating $MyHC^+$ cells and the fusion index were both markedly reduced, with only myocytes or small myotubes present (Figure 7b and e). Consistent with these observations, western blot analysis revealed a slight decrease in myogenin levels (Figure 7f). We also found that the fusion defect induced by Noggin knockdown could be rescued by Dorsomorphin-mediated blockade of intracellular BMP signalling (Figure 7g, quantified h), indicating that endogenous Noggin from differentiating cells is required for proper myotube formation, through suppression of BMP signalling.

BMP signalling is operative during muscle regeneration *in vivo*. Finally, we evaluated whether BMP signalling was also operative in satellite cells in regenerating muscle *in vivo*. Cardiotoxin was used to induce damage in the gastrocnemius muscle of adult mice. After 3 days, the regenerating muscles were removed, cryosectioned and immunostained for pSmad1/5/8, together with MyoD, to identify satellite cell-derived myoblasts: 97.4 ± 2.9% ($n=50$ cells from each of 3 mice) of $MyoD^+$ cells contained pSmad1/5/8 (Figure 8a). Undamaged areas of the muscle periphery provided the control and no pSmad1/5/8 immunostaining was associated with myofibres in these non-regenerating regions (data not shown).

Regenerating gastrocnemius muscle was also injected with either 50 μl of 10 μM Dorsomorphin (Figure 8b–d) or 50 μl of 100 μg/ml sBMPR-1Af (Figure 8e–g) at 1 and 3 days after cardiotoxin-induced injury. The contralateral regenerating muscle served as the control and was injected with 50 μl of vehicle. Regenerating muscles were removed on day 8 and immunostained for MyHC and collagen type 1 (Figure 8b and e). Administration of Dorsomorphin resulted in a significant ~20% decrease in the mean perimeter of centrally nucleated regenerating myofibres compared with controls, whereas the reduction was nearer ~40% with sBMPR-1Af (Figure 8c and f). A significant ~1.5-fold increase in collagen type 1 deposition after either Dorsomorphin or sBMPR-1Af administration was also observed (Figure 8d and g).

Discussion

In this study, we investigated the role of BMP signalling in normal adult myogenesis. We found that exogenous BMP4 was able to sustain proliferation in satellite cells and inhibit differentiation. Conversely, blocking interaction of BMP with

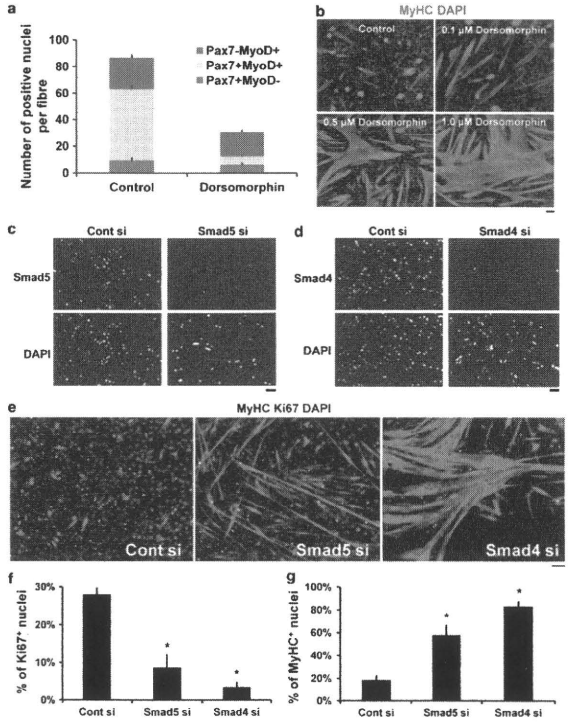

Figure 5 Inhibiting intracellular BMP signal mediation promotes myogenic differentiation. To inhibit BMP signaling, we used either Dorsomorphin, an inhibitor of Smad1/5/8 phosphorylation, or siRNA to knockdown the R-Smad, Smad5, or Co-Smad, Smad4, levels. (**a**) EDL myofibres and their associated satellite cells were cultured with or without 1 μM Dorsomorphin and the plating medium changed daily. Dorsomorphin markedly decreased the mean total number of cells per fibre, particularly the number of cells with the Pax7$^+$ MyoD$^+$ phenotype. (**b**) Satellite cell-derived myoblasts were plated at high cell density (80–90% confluency) and cultured in proliferation medium for 2 days with or without Dorsomorphin. Immunostaining for MyHC showed that Dorsomorphin promoted myogenic differentiation and fusion in a dose-dependent manner. (**c** and **d**) Efficient siRNA-mediated knockdown of Smad5 or Smad4 was confirmed by immunostaining of plated satellite cells 24 h after transfection. (**e**, quantified in **f** and **g**) Co-immunostaining for MyHC and Ki67 after Smad5 or Smad4 silencing for 3 days in proliferation medium was sufficient to promote cell cycle exit and induce precocious differentiation, characterised by a decreased proportion of cells with Ki67$^+$ expression and an increase in MyHC$^+$ cells and myotubes. Data are mean ± S.E.M. (**a**) or mean ± S.D. (**f** and **g**) from at least three independent experiments. Asterisk indicates that data are significantly different from control conditions ($P<0.05$). Scale bar equals 50 μm

its receptors, downregulating BMPR-1A or perturbing intracellular BMP signal mediation, all induced rapid differentiation. Thus, BMP signalling initially serves to allow expansion of the satellite cell pool by stimulating proliferation and preventing precocious myogenic differentiation (Figure 9).

The source of BMPs that act on satellite cells *in vivo* remains to be determined, but myogenic cells can express and secrete BMP4,[29,30] with higher levels produced by myoblasts from dystrophic muscle.[31] Additionally, muscle damage may also expose satellite cells to BMP4 in serum,[23] and/or from cells such as macrophages, as microglia/macrophages produce BMPs after CNS damage.[32] Although prolonged exposure of myogenic cells to high levels of BMPs can induce expression of various osteogenic genes,[16] we found that satellite cells exposed to BMP4 for shorter periods, likely encountered during muscle repair/regeneration *in vivo*, did not obviously compromise their myogenic identity.

Satellite cells respond to BMPs because they express BMPR-1A, which was undetectable on most quiescent satellite cells, but upregulated as cells were activated. An early event in satellite cell activation is induction of MyoD, which can bind to the promoter of *BMPR-1A* to enhance its expression, and MyoD overexpression leads to BMPR-1A induction.[33] Thus upregulation of BMPR-1A is part of the response of satellite cells to serum stimulation, and siRNA-mediated knockdown of BMPR-1A induced premature differentiation, showing that BMP signalling operates through BMPR-1A. Consistent with our observations, a dominant-negative BMPR-1A mutant enhanced myogenic differentiation in C2 cells maintained in high-serum medium, but a dominant-negative BMPR-1B mutant did not.[23] In contrast, we found that a caBMPR-1A[28] reduced the activity of a *CKM*

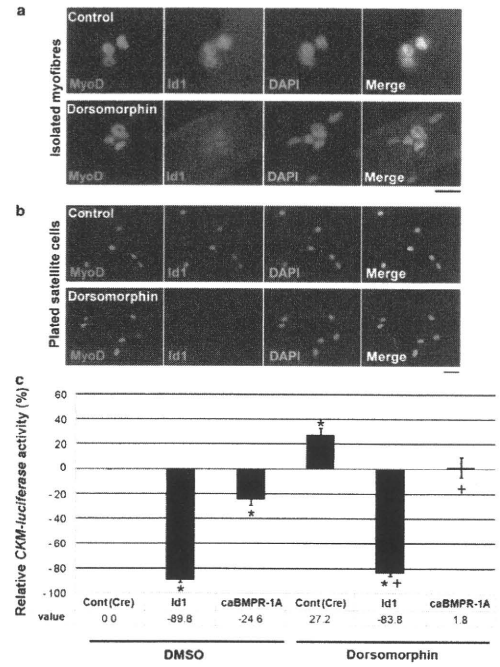

Figure 6 BMP signalling regulates the MyoD-controlled *CKM* promoter. Id1 is a target gene of BMP signalling and a negative regulator of MyoD activity. (**a**) Exposure to 3 μM Dorsomorphin for 6 h to inhibit BMP signalling resulted in a downregulation of Id1 expression in satellite cells associated with a myofibre. (**b**) Similarly, immunostaining of plated satellite cells after exposure to 3 μM Dorsomorphin for 18 h in proliferation medium also resulted in downregulation of Id1 protein. Scale bar equals 20 μm. (**c**) To investigate the ability of MyoD to activate its transcriptional targets, plated satellite cell-derived myoblasts were transfected with a *CKM* (muscle creatine kinase) Luciferase reporter plasmid (*CKM-LUCpCS2*), whose activity is regulated by MyoD, together with a *Renilla* luciferase plasmid *pRL* driven by a minimal *tk promoter*, as an internal control. Plated satellites cells were co-transfected with either *Cre*-expressing control plasmid or *Id1*-expressing plasmid or constitutively active *BMPR-1A* (*caBMPR-1A*)-expressing plasmid, together with *CKM-LUCpCS2*. After transfection, the cells were cultured in proliferation medium with or without 5 μM Dorsomorphin for 24 h before reporter assay. Id1 or caBMPR-1A reduced *CKM-LUCpCS2* activity. In contrast, inhibition of BMP signalling with Dorsomorphin had the opposite effect, and increased *CKM-LUCpCS2* activity. Both Id1 and caBMPR-1A were able to reverse this increase in *CKM-LUCpCS2* activity produced by exposure to Dorsomophin. Data are represented as mean ± S.D. from at least three independent experiments. Asterisk denotes that data are significantly different from control conditions, whereas a cross indicates that data are different from the level of *CKM-LUCpCS2* activity in the presence of Dorsomorphin ($P<0.05$), using Student's *t*-test

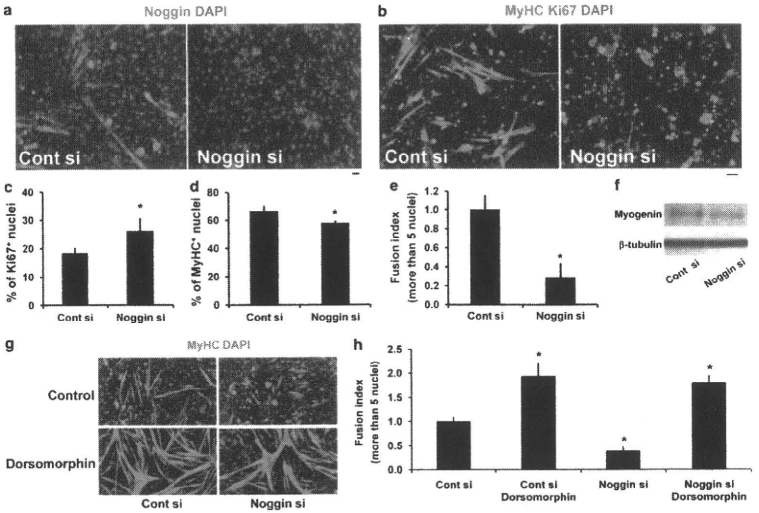

Figure 7 Reducing Noggin levels enhances satellite cell proliferation but inhibits differentiation. To further understand the role of Noggin in myogenic progression, we used siRNA-mediated knockdown of Noggin protein. (**a**) Efficient Noggin knockdown in plated satellite cell-derived myoblasts was confirmed by immunostaining for Noggin 3 days after siRNA (Noggin si) transfection. (**b**, quantified in **c**–**e**) The effects of Noggin knockdown were analysed by co-immunostaining for MyHC and Ki67, which revealed an increase in myoblast proliferation, but a reduction in differentiation and fusion into large myotubes. (**f**) Western blotting also showed that Noggin siRNA reduced myogenin levels in plated satellite cells. (**g**, quantified in **h**) The effect of Dorsomorphin (1 μM) treatment to inhibit BMP signalling on Noggin siRNA-transfected cells was analysed by immunostaining for MyHC. Dorsomorphin reversed the fusion defect induced by Noggin knockdown. Mean ± S.D. from at least three independent experiments is shown. Asterisk indicates that data are significantly different from control ($P<0.05$) using paired one-tail *t*-test. Scale bar equals 30 μm

reporter that is normally upregulated during myogenic differentiation.

BMPs are known to control the ability of MyoD to transactivate its target genes by Smad-mediated regulation of Id proteins,[6–8] negative regulators of MyoD function and terminal differentiation.[9,27] Proliferating satellite cell-derived myoblasts contain both MyoD and Id1, with Id1 presumably curtailing MyoD function to prevent premature differentiation. Id1 levels are then dramatically reduced as satellite cells undergo differentiation.[25] Consistent with these observations, although Id1 and Id3 are undetectable in muscle lysates from uninjured muscle, they are upregulated during muscle regeneration, peaking around day 3.[30] In satellite cells, we found that inhibiting BMP signalling reduced Id1 levels, promoted differentiation and increased *CKM* promoter activity.

Delta/Notch signalling permits satellite cell expansion and prevents precocious differentiation.[34] Notch signalling is required for BMP4 to impede myogenic differentiation in C2 cells: inhibitors of γ-secretase prevent cleavage of Notch to release the active intracellular domain and can partially reverse the BMP-induced differentiation block.[18] The catalytic subunit of the γ-secretase complex is presenilin-1, and we recently showed that presenilin-1 can inhibit satellite cell differentiation through both γ-secretase-dependent and γ-secretase-independent mechanisms.[25] The γ-secretase-dependent effects of presenilin-1 on impeding differentiation are likely through controlling Notch signalling. Crucially, however, the γ-secretase (Notch)-independent presenilin-1 mechanism operates by augmenting Pax7 and controlling Id1 levels,[25] and intriguingly, Id1, Id2 and Id3 are direct transcriptional targets of Pax7.[29] This γ-secretase-independent mechanism is unlikely to work through BMP signalling, however, as there is no difference in pSmad1/5/8 levels between *presenilin-1*-null or control embryonic fibroblasts transfected with MyoD, even though only the MyoD-expressing *presenilin-1*-null cells readily differentiate in high-serum medium (unpublished observations). Furthermore, overexpression of Wnt3a in C2 cells is capable of overcoming the BMP2-mediated block of differentiation by downregulating Id1.[35] Thus γ-secretase-independent presenilin-1 signalling and the BMP pathway both seem to separately converge on Ids to regulate satellite cell function.

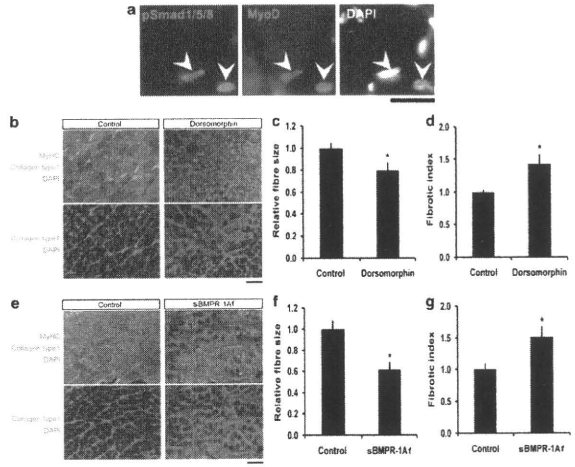

Figure 8 BMP signalling operates during normal muscle regeneration *in vivo*. Regeneration was induced in mouse gastrocnemius muscles by injection of cardiotoxin. (**a**) Satellite cell-derived myoblasts, identified by MyoD expression, also expressed pSmad1/5/8 (arrowheads) in regenerating muscle on day 3 of regeneration. (**b**–**g**) To examine the effects of blockade of BMP signalling, 50 μl of 10 μM Dorsomorphin/DMSO in saline or 50 μl of 100 μg/ml sBMPR-1Af were intramuscularly injected into the right gastrocnemius, 1 and 3 days after cardiotoxin injection. Regenerating left gastrocnemius served as a control and received vehicle alone (DMSO/saline for Dorsomorphin or BSA solution for sBMPR-1Af). Muscle regeneration was assayed by immunostaining cryosections for MyHC and collagen type 1. (**b**, **c**, **e** and **f**) Treatment with either Dorsomorphin or sBMPR-1Af resulted in a significant decrease in the mean perimeter of centrally nucleated regenerating myofibres, compared with controls (100 regenerating fibres in the regenerating area of each animal were measured, and the mean size after exposure to Dorsomorphin or sBMPR-1Af expressed as the proportional change compared with the mean size of control regenerating myofibres). (**b**, **d**, **e** and **g**) Immunostaining for collagen type 1 was used to measure the degree of endomysial fibrosis, and a significant increase in the fibrotic index was observed in muscles exposed to either Dorsomorphin or sBMPR-1Af, compared with controls (the area of collagen type 1 expression in the regenerating area was measured in 1–3 sections for each animal, using ImageJ and changes with exposure to Dorsomorphin or sBMPR-1Af expressed as fold-difference compared with control). Six mice were used for each condition. Data are mean ± S.E.M., where an asterisk denotes a significant difference from control ($P<0.05$). Scale bars equal 100 μm

Antagonism of BMP signalling by Noggin is employed during development to protect pre-myogenic cells, and expansion of the Noggin expression domain promotes ectopic myogenesis.[11,12] We found that Noggin-mediated interference with BMP signalling was also redeployed during adult myogenesis. Noggin was upregulated as satellite cells differentiated, and knocking down Noggin resulted in more cells proliferating, while fewer differentiated. As Noggin is a secreted signalling molecule, it may also act in a paracrine manner to reduce BMP signalling in proliferating cells to potentiate and augment timely differentiation. Noggin expression in C2 cells is upregulated by exogenous BMP2,[36] and administration of Noggin to regenerating muscle reduces both pSmad1/5/8 and Id1 levels.[30] In addition, rhabdomyosarcoma cells express myogenic genes including MyoD and myogenin but form myotubes poorly, and have relatively high levels of *BMP4* and lower expression of *Noggin* than primary myoblasts.[37] Furthermore, specification of myogenic cells is unaffected in *Noggin*-null embryos, but differentiation is clearly perturbed, with meagre myotube formation during foetal myogenesis,[38] again suggesting a common role for Noggin in supporting differentiation in both developmental and adult myogenesis.

We observed that inhibition of BMP signalling during muscle regeneration resulted in smaller regenerated myofibres. Similarly, *Id1*$^{-/+}$ *Id3*$^{-/-}$ mice also exhibit a muscle regeneration defect, with the cross-sectional area of regenerated myofibres being only ~50% of wild type.[30] These mice also had fewer proliferating satellite cells during regeneration.[30]

In conclusion, BMP signalling is part of the programme that regulates routine satellite cell function. BMPs stimulate proliferation and prevent precocious differentiation to allow amplification of satellite cell-derived myoblasts. Noggin is then upregulated as satellite cell progeny differentiate, to antagonise BMP signalling and facilitate coordinated differentiation (Figure 9).

Materials and Methods

Isolation and culture of primary satellite cells and myoblasts. Adult (8–12 weeks old) C57BL10 mice were killed by cervical dislocation, and the EDL (or masseter for Figure 3b only) muscle isolated and

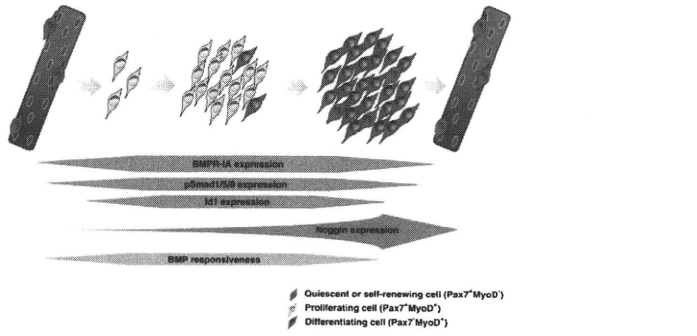

Figure 9 Role of BMP signalling during myogenic progression in satellite cells. During muscle repair and regeneration, quiescent Pax7 $^+$ satellite cells are activated to co-express Pax7 and MyoD. Satellite cell-derived myoblasts proliferate extensively before many cells then downregulate Pax7 and differentiate to either repair damaged muscle fibres or fuse together to generate new myofibres. Other satellite cells maintain Pax7 expression but lose MyoD, and self-renew to maintain a viable stem cell compartment. Normal BMP signalling through BMPR-1A and Smad1/5/8 phosphorylation is required during muscle repair/regeneration to allow the satellite cell-derived myoblast population to expand, by preventing precocious differentiation. BMP signalling operates through controlling Id levels, a negative regulator of MyoD and myogenic differentiation. As satellite cell progeny differentiate, Noggin is upregulated to antagonise the BMP signal, so facilitating the myogenic differentiation programme

digested in collagenase type1, as previously described.[25] Most satellite cells are mitotically quiescent in healthy adult muscle, so must first be activated and will then enter the cell cycle.[2] To induce satellite cell activation *in vitro*, myofibers and associated satellite cells were cultured in plating medium (DMEM supplemented with L-glutamine or GlutaMax (Sigma, Poole, Dorset, UK), 10% horse serum (PAA Laboratories, Yeovil, Somerset, UK), 0.5% chicken embryonic extract (MTX Lab Systems, Vienna, VA, USA) and 1% penicillin–streptomycin (Sigma)) at 37°C in 5% CO_2, as described previously.[24] To prepare plated satellite cells, either cells were removed from myofibers by enzymatic treatment with 0.125% trypsin–EDTA (Sigma) for 10 min at 37°C or allowed to migrate from isolated myofibres cultured on Matrigel. Satellite cells were then re-plated on Matrigel at equal density and maintained in proliferation medium (DMEM supplemented with L-glutamine or GlutaMAX, 20–30% foetal bovine serum, 1% chicken embryo extract, 10 ng/ml bFGF and 1% penicillin–streptomycin). Satellite cells were treated with 100 ng/ml recombinant BMP4 protein, (Peprotech, London, UK), 50 ng/ml recombinant Noggin protein (Peprotech), 200 ng/ml sBMPR-1Af (R&D systems, Abingdon, Oxfordshire, UK) or 0.1–3 μM Dorsomorphin (also known as Compound C; Calbiochem-MERCK-Beeston, Nottingham, UK) administered to the culture medium. In other experiments, satellite cells were switched from proliferation medium to differentiation medium (DMEM with L-glutamine or GlutaMax and supplemented with 2% horse serum and 1% penicillin–streptomycin) and cultured for 48 h with or without BMP4 (200 ng/ml). Myofibres and associated satellite cells or plated satellite cells were fixed with warm 4% paraformaldehyde (PFA).

Antibodies used in the study. Antibodies were obtained from the following sources. Rabbit anti-BMPR-1A (Alk-3) from Orbigen (San Diego, CA, USA) and a gift from Professor B. Kay;[39] rat anti-Ki67 from DakoCytomation (Ely, Cambridgeshire, UK); goat anti-Smad5, mouse anti-Smad4, mouse anti-MyoD and rabbit anti-MyoD antibodies were obtained from Santa Cruz (Santa Cruz, USA); goat anti-Noggin antibody was obtained from R&D systems; mouse anti-MyHC (MF20), anti-Pax7, anti-myogenin (F5D) and anti-β-tubulin antibodies (E7) were supplied by the DSHB (Iowa City, IA, USA); rabbit anti-pSmad1/5/8 antibody was from Cell Signalling Technology (Beverly, MA, USA); goat anti-collagen type 1 antibody was acquired from Southern Biotech (Birmingham, AL, USA). Mounting medium containing 4,6-diamidino-2-phenylindole (DAPI) to counterstain all nuclei and the M.O.M kit were both purchased from Vector Laboratories, Orton Southgate, Peterborough, UK.

Immunoblot analysis. Immunoblot analysis was performed as previously described.[25] Anti-BMPR-1A, anti-MyHC, anti-Pax7, anti-Myogenin or anti-β-tubulin antibodies were applied in PBS containing 0.1% Tween20 and incubated at 4°C overnight. HRP-conjugated secondary antibodies were used for visualisation by chemiluminescence (Fujifilm, Bedford, UK).

Immunostaining. Immunocytochemistry was as previously described.[25] Anti-BMPR-1A, anti-Ki67, anti-Smad5, anti-Smad4, anti-MyoD, anti-Noggin, anti-MyHC, anti-Pax7, anti-myogenin, anti-Id1 or anti-pSmad1/5/8 antibodies were applied at 4°C overnight. For co-immunostaining sections, frozen regenerating muscle cross-sections were fixed with 4% PFA, blocked using the M.O.M kit and incubated with either anti-pSmad1/5/8 and anti-MyoD antibodies or with anti-MyHC and anti-collagen type 1 antibodies. Immunostained myofibres, plated cells or cryosections were viewed on a Zeiss Axiophot 200M using Plan-Neofluar lenses (Zeiss, Welwyn Garden City, Hertfordshire, UK), or on a Nikon (Kingston upon Thames, Surrey, UK) C1si confocal using Plan-Fluor lenses. Digital images were acquired with a Zeiss AxioCam HRm Charge-Coupled Device using AxioVision software version 4.4. Images were optimised globally and assembled into figures using Adobe Photoshop. The Click-iT Tunel Alexa fluor imaging assay (Invitrogen, Life Technologies, Paisley, UK) was used as per the manufacturer's instructions on satellite cells cultured for 24 h in proliferation medium containing either 1 μM or 5 μM Dorsomorphin ($n = 3$ mice).

***CKM-luciferase* reporter assay.** Plated satellite cells were co-transfected with the *CKM firefly Luciferase* reporter plasmid (*CKM-LUCpCS2*) and *pcDNA3-Cre*-expressing control vector, *pcDNA3-mId1*-expressing vector[27] or *pcDEF3-caBMPR-1A*-expressing vector,[7] using Lipofectamine LTX according to the manufacturer's instructions. The *Renilla* luciferase plasmid *pRL* (Promega Corporation, Madison, WI, USA), driven by a minimal tk promoter, was included as an internal control. Dorsomorphin was added to a final concentration of 5 μM. At 48 h post-transfection, the dual-Luciferase reporter assay (Promega) was performed according to the manufacturer's instructions and measured on an Anthos Lucy3 (JENCONS-PLS, East Grinstead, West Sussex, UK).

siRNA-mediated gene knockdown. The transfection of siRNA (Invitrogen Life Technologies) into primary satellite cell-derived myoblasts was performed using Lipofectamine 2000 reagent (Invitrogen Life Technologies) or Lipofectamine RNAiMAX (Invitrogen Life Technologies) as previously described.[25] Transfection of siRNA into single myofibers was carried out 12–16 h after isolation with Lipofectamine RNAiMAX (Invitrogen Life Technologies).[25] All samples were examined 1–3 days after the transfection. The following siRNA sequences were used: BMPR-1A siRNA: 5′-GAAGUGCUGGAUGAAAGCCUGAAUA-3′, Smad4 siRNA: 5′-GGAGAGACGUUUAAGGUCCCUUCAA-3′, Smad5 siRNA: 5′-CCUG GGAUUGUUGUCAAAUGUUAAU-3′ and Noggin siRNA: 5′-CGACCCGGG CUUUAUGGCUACUUCG-3′. Control siRNAs were supplied by Invitrogen Life Technologies.

Muscle regeneration studies. Animal husbandry, breeding and experimental procedures were passed by the Ethical Review Process Committee of the King's College London, and were carried out in accordance with British law under the provisions of the Animals (Scientific Procedures) Act 1986. To assay pSmad1/5/8 expression, the gastrocnemius muscle of 10-week-old male C57BL/10 mice was injected with 50 μl of 10 μM cardiotoxin (Sigma) using a 29-G 1/2 insulin syringe. Muscles were removed 3 days later and immediately frozen in isopentane cooled in liquid nitrogen, and stored at −80°C before being cryosectioned and immunostained for pSmad1/5/8 and MyoD. To assay regenerative capacity in the presence of perturbed BMP signalling, the belly of both the left and right gastrocnemius muscles of 7- to 9-week-old male C57BL/10 mice were injected with 25 μl of 10 μM cardiotoxin (Sigma). At 1 and 3 days after cardiotoxin injection, 50 μl of 10 μM Dorsomorphin/DMSO dissolved in saline or 50 μl of 100 μg/ml sBMPR-1Af dissolved in saline, were injected intramuscularly into the right gastrocnemius muscle at the same site as the cardiotoxin. Control solutions (same concentration of DMSO dissolved in saline for Dorsomorphin or BSA dissolved in saline for sBMPR-1Af) were injected into the left muscle as a control. Muscles were removed 8 days after cardiotoxin injection and immediately frozen in isopentane cooled in liquid nitrogen and stored at −80°C Transverse sections of muscle were cut with a cryostat and co-immunostained for MyHC and collagen type 1. Measurement of centrally nucleated regenerating myofibres and the area of endomysial fibrosis was performed using ImageJ software (developed by NIH and available for free download at http://rsb.info.nih.gov/ij).

Statistical analysis. Data are presented as mean ± standard deviation (S.D.) or mean ± standard error (S.E.M.). Immunostained satellite cells from at least 10 myofibres were scored from each of at least three mice for each experiment. Significant differences between test conditions and controls were determined using Student *t*-test, wherein *P*-values < 0.05 were considered to be statistically significant.

Conflictal of interest

The authors declare no conflict of interest.

Acknowledgements. We thank Dr. Stephen J. Tapscott for providing the *CKM-LUCpCS2* reporter plasmid; Dr. Robert Benezra for generously sharing *pcDNA3-mId1* construct; Dr. Naohiro Hashimoto for helpful discussions and Paul Knopp for much help. We gratefully acknowledge colleagues who shared antibodies, including through the Developmental Studies Hybridoma Bank developed under the auspices of the NICHD and maintained by the University of Iowa. Y.O. was funded by the Muscular Dystrophy Campaign (RA3/737); F.C. is sponsored by the Association of International Cancer Research (07-0151); J.E.M. is backed by a Wellcome Trust university award. The laboratory of P.S.Z. is also supported by The Wellcome Trust, The Medical Research Council, the MYORES Network of Excellence (contract 511978) from the European Commission 6th Framework Programme and the collaborative Project OPTISTEM (Grant Agreement number: 223098) from the European Commission 7th Framework Programme.

1. Zammit PS. All muscle satellite cells are equal, but are some more equal than others? *J Cell Sci* 2008; **121**: 2975–2982.
2. Zammit PS, Golding JP, Nagata Y, Hudon V, Partridge TA, Beauchamp JR. Muscle satellite cells adopt divergent fates: a mechanism for self-renewal? *J Cell Biol* 2004; **166**: 347–357.
3. Halevy O, Piestun Y, Allouh MZ, Rosser BW, Rinkevich Y, Reshef R *et al.* Pattern of Pax7 expression during myogenesis in the posthatch chicken establishes a model for satellite cell differentiation and renewal. *Dev Dyn* 2004; **231**: 489–502.
4. Collins CA, Olsen I, Zammit PS, Heslop L, Petrie A, Partridge TA *et al.* Stem cell function, self-renewal, and behavioral heterogeneity of cells from the adult muscle satellite cell niche. *Cell* 2005; **122**: 289–301.
5. Feng XH, Derynck R. Specificity and versatility in TGF-beta signaling through Smads. *Annu Rev Cell Dev Biol* 2005; **21**: 659–693.
6. Hollnagel A, Oehlmann V, Heymer J, Ruther U, Nordheim A. Id genes are direct targets of bone morphogenetic protein induction in embryonic stem cells. *J Biol Chem* 1999; **274**: 19838–19845.
7. Katagiri T, Imada M, Yanai T, Suda T, Takahashi N, Kamijo R. Identification of a BMP-responsive element in Id1, the gene for inhibition of myogenesis. *Genes Cells* 2002; **7**: 949–960.
8. Korchynskyi O, ten Dijke P. Identification and functional characterization of distinct critically important bone morphogenetic protein-specific response elements in the Id1 promoter. *J Biol Chem* 2002; **277**: 4883–4891.
9. Jen Y, Weintraub H, Benezra R. Overexpression of Id protein inhibits the muscle differentiation program: *in vivo* association of Id with E2A proteins. *Genes Dev* 1992; **6**: 1466–1479.
10. Wozney JM, Rosen V, Celeste AJ, Mitsock LM, Whitters MJ, Kriz RW *et al.* Novel regulators of bone formation: molecular clones and activities. *Science* 1988; **242**: 1528–1534.
11. Reshef R, Maroto M, Lassar AB. Regulation of dorsal somitic cell fates: BMPs and Noggin control the timing and pattern of myogenic regulator expression. *Genes Dev* 1998; **12**: 290–303.
12. Réem-Kalma Y, Lamb T, Frank D. Competition between noggin and bone morphogenetic protein 4 activities may regulate dorsalization during Xenopus development. *Proc Natl Acad Sci USA* 1995; **92**: 12141–12145.
13. Hirsinger E, Duprez D, Jouve C, Malapert P, Cooke J, Pourquie O. Noggin acts downstream of Wnt and Sonic Hedgehog to antagonize BMP4 in avian somite patterning. *Development* 1997; **124**: 4605–4614.
14. Amthor H, Christ B, Weil M, Patel K. The importance of timing differentiation during limb muscle development. *Curr Biol* 1998; **8**: 642–652.
15. Wada MR, Inagawa-Ogashiwa M, Shimizu S, Yasumoto S, Hashimoto N. Generation of different fates from multipotent muscle stem cells. *Development* 2002; **129**: 2987–2995.
16. Katagiri T, Yamaguchi A, Komaki M, Abe E, Takahashi N, Ikeda T *et al.* Bone morphogenetic protein-2 converts the differentiation pathway of C2C12 myoblasts into the osteoblast lineage. *J Cell Biol* 1994; **127**: 1755–1766.
17. Asakura A, Komaki M, Rudnicki M. Muscle satellite cells are multipotential stem cells that exhibit myogenic, osteogenic, and adipogenic differentiation. *Differentiation* 2001; **68**: 245–253.
18. Dahlqvist C, Blokzijl A, Chapman G, Falk A, Dannaeus K, Ibanez CF *et al.* Functional Notch signaling is required for BMP4-induced inhibition of myogenic differentiation. *Development* 2003; **130**: 6089–6099.
19. Kaplan FS, Shen Q, Lounev V, Seemann P, Groppe J, Katagiri T *et al.* Skeletal metamorphosis in fibrodysplasia ossificans progressiva (FOP). *J Bone Miner Metab* 2008; **26**: 521–530.
20. Lounev VY, Ramachandran R, Wosczyna MN, Yamamoto M, Maidment AD, Shore EM *et al.* Identification of progenitor cells that contribute to heterotopic skeletogenesis. *J Bone Joint Surg Am* 2009; **91**: 652–663.
21. Yu PB, Deng DY, Lai CS, Hong CC, Cuny GD, Bouxsein ML *et al.* BMP type I receptor inhibition reduces heterotopic ossification. *Nat Med* 2008; **14**: 1363–1369.
22. Namiki M, Akiyama S, Katagiri T, Suzuki A, Ueno N, Yamaji N *et al.* A kinase domain-truncated type I receptor blocks bone morphogenetic protein-2-induced signal transduction in C2C12 myoblasts. *J Biol Chem* 1997; **272**: 22046–22052.
23. Kodaira K, Imada M, Goto M, Tomoyasu A, Fukuda T, Kamijo R *et al.* Purification and identification of a BMP-like factor from bovine serum. *Biochem Biophys Res Commun* 2006; **345**: 1224–1231.
24. Ono Y, Boldrin L, Knopp P, Morgan JE, Zammit PS. Muscle satellite cells are a functionally heterogeneous population in both somite-derived and branchiomeric muscles. *Dev Biol* 2010; **337**: 29–41.
25. Ono Y, Gnocchi VF, Zammit PS, Nagatomi R. Presenilin-1 acts via Id1 to regulate the function of muscle satellite cells in a gamma-secretase-independent manner. *J Cell Sci* 2009; **122**: 4427–4438.
26. Yu PB, Hong CC, Sachidanandan C, Babitt JL, Deng DY, Hoyng SA *et al.* Dorsomorphin inhibits BMP signals required for embryogenesis and iron metabolism. *Nat Chem Biol* 2008; **4**: 33–41.
27. Benezra R, Davis RL, Lockshon D, Turner DL, Weintraub H. The protein Id: a negative regulator of helix-loop-helix DNA binding proteins. *Cell* 1990; **61**: 49–59.
28. Akiyama S, Katagiri T, Namiki M, Yamaji N, Yamamoto N, Miyama K *et al.* Constitutively active BMP type I receptors transduce BMP-2 signals without the ligand in C2C12 myoblasts. *Exp Cell Res* 1997; **235**: 362–369.
29. Kumar D, Shadrach JL, Wagers AJ, Lassar AB. Id3 is a direct transcriptional target of Pax7 in quiescent satellite cells. *Mol Biol Cell* 2009; **20**: 3170–3177.
30. Clever JL, Sakai Y, Wang RA, Schneider D. Inefficient skeletal muscle repair in inhibitor of differentiation (Id) knockout mice suggests a crucial role for bmp signaling during adult muscle regeneration. *Am J Physiol Cell Physiol* 2010; **298**: C1087–C1099.
31. Sterrenburg E, van der Wees CG, White SJ, Turk R, de Menezes RX, van Ommen GJ *et al.* Gene expression profiling highlights defective myogenesis in DMD patients and a possible role for bone morphogenetic protein 4. *Neurobiol Dis* 2006; **23**: 228–236.

32. Xiao Q, Du Y, Wu W, Yip HK. Bone morphogenetic proteins mediate cellular response and, together with Noggin, regulate astrocyte differentiation after spinal cord injury. *Exp Neurol* 2010; **221**: 353–366.
33. Liu R, Ginn SL, Lek M, North KN, Alexander IE, Little DG *et al*. Myoblast sensitivity and fibroblast insensitivity to osteogenic conversion by BMP-2 correlates with the expression of Bmpr-1a. *BMC Musculoskelet Disord* 2009; **10**: 51.
34. Conboy IM, Rando TA. The regulation of Notch signaling controls satellite cell activation and cell fate determination in postnatal myogenesis. *Dev Cell* 2002; **3**: 397–409.
35. Nakashima A, Katagiri T, Tamura M. Cross-talk between Wnt and bone morphogenetic protein 2 (BMP-2) signaling in differentiation pathway of C2C12 myoblasts. *J Biol Chem* 2005; **280**: 37660–37668.
36. Takayama K, Suzuki A, Manaka T, Taguchi S, Hashimoto Y, Imai Y *et al*. RNA interference for noggin enhances the biological activity of bone morphogenetic proteins *in vivo* and *in vitro*. *J Bone Miner Metab* 2009; **27**: 402–411.
37. Goldstein M, Meller I, Orr-Urtreger A. FGFR1 over-expression in primary rhabdomyosarcoma tumors is associated with hypomethylation of a 5′ CpG island and abnormal expression of the AKT1, NOG, and BMP4 genes. *Genes Chromosomes Cancer* 2007; **46**: 1028–1038.
38. Tylzanowski P, Mebis L, Luyten FP. The Noggin null mouse phenotype is strain dependent and haploinsufficiency leads to skeletal defects. *Dev Dyn* 2006; **235**: 1599–1607.
39. Kariyawasam HH, Xanthou G, Barkans J, Aizen M, Kay AB, Robinson DS. Basal expression of bone morphogenetic protein receptor is reduced in mild asthma. *Am J Respir Crit Care Med* 2008; **177**: 1074–1081.

特集　薬剤性神経疾患

悪性症候群*

久野貞子**[1]

Key Words：neuroleptic malignant syndrome, neuroleptica, anti-parkinsonian drugs, Parkinson's disease

悪性症候群とは

悪性症候群（neuroleptic malignant syndrome, *syndrome malin*）は抗精神病薬，抗Parkinson病（PD）薬など中枢神経系に作用する向精神薬の服用や中止に関連して発症する副作用であり，ドパミンD2受容体遮断性抗精神病薬の増量中やドパミン作動性抗PD薬の中止で起こることが知られている．通常，38℃以上の非感染性発熱，頻脈，血圧の変動，意識障害，パーキンソニズム（無動，筋強剛，振戦など）をきたし，適切な処置をせずに放置すると死亡する重篤な副作用であることから悪性症候群と名づけられている．歴史的には，1950年代初期に強力な抗精神病薬としてchlorpromazineが臨床応用され，1950年代後半に悪性症候群様の疾患が報告され，抗精神病薬との関連が問題とされてきた．1960年代になってDelay & Deniker[1]が*syndrome malin*と提唱したとされ，当時は「稀ではあるが，もっとも重篤な抗精神病薬の副作用」とされていた．悪性症候群の頻度は発表者や対象によって異なるが，Bertorini[2]は，抗精神病薬治療を受けている患者の0.5～2.4%に発症するとしているが，最近の研究では発症率は抗精神病薬使用者の0.2～1.0%であろうと報告されている．わが国では1986年から1987年に厚生省研究班が行った調査[3]では，回答した施設の68.9%が悪性症候群を経験したことがあると報告している．一方，抗PD薬の中止に関連した悪性症候群は，1970年以降治療薬のgold standardとされるL-dopaやアマンタジンが臨床に導入されてから報告されるようになり[4][5]，1980年代後半から悪性症候群の発現に対する注意が喚起され[6]，重篤例が減少している．

本稿では悪性症候群一般について記述し，さらに神経内科医が遭遇することが多い抗PD薬投与中または中止による悪性症候群について，自験症例での経験を中心に診断，対処法，予防などについても記載する．

悪性症候群を起こす可能性のある薬剤

1）抗てんかん剤：カルバマゼピン．

2）抗PD剤：塩酸アマンタジン，ドロキシドパ，レボドパ，レボドパ配合剤，COMT阻害剤．

3）精神神経用剤－フェノチアジン系：塩酸クロルプロマジン，塩酸クロルプロマジン配合剤，レボメプロマジン，ペルフェナジン，マレイン酸ペルフェナジン，マレイン酸フルフェナジン，塩酸フルフェナジン，フェンジゾ酸ペルフェナジン，マレイン酸トリフロペラジン，マレイン酸プロクロルペラジン，塩酸チオリダジン，ジメタンスルホン酸チオプロペラジン，プロペリシアジン．

4）精神神経用剤－ブチロフェノン系製剤：ハロペリドール，チミペロン，ブロムペリドール，塩酸ビパンペロン，スピペロン，塩酸モペロン．

5）精神神経用剤－三環系抗うつ剤：塩酸イミプラミン，塩酸アミトリプチン，塩酸クロミプラミン，塩酸デシプラミン，マレイン酸トリミプラミン，塩酸ノルトリプチリン，塩酸ロフェプラミン，アモキサピン，塩酸ドスレピン．

6）精神神経用剤－四環系抗うつ剤：塩酸マプロチリン，塩酸ミアンセリン，マレイン酸セチプチリン．

7）精神神経用剤－リチウム製剤：炭酸リチウム．

8）精神神経用剤－その他：ピモジド，塩酸カルピプラミン，クロルプロチキセン，塩酸クロカプラミン，塩酸モサプラミン，オキシペルチン，チオチキセン，スルピリド，塩酸スルトプリド，ネモナプリド，ゾテピン．

9）その他の中枢神経系用剤：塩酸チアプリド．

10）その他の消化器官用剤：メトクロプラミド．

悪性症候群の症状

悪性症候群の典型的な発症は，前駆症状としてパーキンソニズム〔無動，筋強剛，振戦（PDでは改善していた運動症状の再燃）〕，発汗，頻脈，流涎，体温上昇などであり，この段階で輸液など適切な処置がされず放置すると悪性症候群に進行し，体温は1～2日の間に38～40℃以上に上昇し，意識障害，急速に進行する脱水症状や栄養・呼吸・循環障害に陥り，ついには死に至ることもある．

悪性症候群の診断

診断は高用量の抗精神病薬を投与しており，それをさらに増量中の患者，低用量であっても高齢者や重篤な全身疾患合併の高リスク患者では感冒や尿路感染など明らかな感染症状が乏しいのに，突如，高熱や血圧変動をきたしたら悪性症候群の可能性を疑うことが診断の第一歩であり，疑わしい場合は直ちに血中CK値や白血球数を測定し，この値が異常に高い場合は悪性症候群疑いと診断する．

悪性症候群の対処法

悪性症候群を疑ったら迅速な対応が不可欠である．抗精神病薬または他の原因医薬品の投与を即時中止し，対症的な全身管理を行いつつ特異的治療を行う．統合失調症などの精神疾患では抗精神病薬の中止により精神症状が急速に悪化する可能性があるが，その場合は一時的に物理的な抑制を行い睡眠薬などで鎮静をはかる．抗PD薬の中止による場合にはいったん中止前の薬剤の投与量に戻し，これらの処置と平行して全身の冷却，輸液などの支持療法を迅速に行う．経口投与が不可能な場合は経静脈的にL-dopa投与を行う．悪性症候群の特異的治療剤としては抗PD薬のブロモクリプチンと末梢性筋弛緩薬のダントロレンの有効性が認められているので，必要に応じて使用する．

PDにおける悪性症候群

1．抗PD薬中断後に発症した悪性症候群

1980年著者らは，PD患者（56歳，男性，罹病期間9年）に発症した悪性症候群を初めて経験した．この患者はL-dopa投与開始約1年後から，しばしば幻視，幻聴，妄想（息子が警察に捕らわれている）などの精神症状が出現していたが自立生活は可能であった．あるとき，図1に示すように患者の強い希望でL-dopa（100mg＋benserazide 25mg）を6.5錠から0.5錠増量後，薬は毒であるという幻聴のため拒薬するようになった．その4日後，高熱，せん妄様意識障害が出現し緊急入院となった．入院後40℃の高熱，発汗過多，皮膚蒼白，意識障害，全身の高度の筋固縮，無動状態が続き，消化管出血もきたしたが，全身の冷却，大量の輸液，点滴内L-dopa投与，抗生物質，副腎皮質ステロイドなどの投与により約2週間後に回復した．しかし，当時はPD薬を継続投与されていた患者の突然薬剤中断によって悪性症候群をきたすことを認識しておらず，血清クレアチンキナーゼ（CK）値の測定はしなかった．

2．抗PD薬の中止や変更を伴わない悪性症候群

PD患者に生ずる場合は抗PD薬の急激な減量に伴って発現するのが一般的であるが，抗PD薬の

* Neuroleptic malignant syndrome.
** Sadako KUNO, M.D., Ph.D.: 国立精神・神経センター病院神経内科〔〒187-8551　東京都小平市小川東町4-1-1〕; Department of Neurology, National Center of Neurology and Psychiatry Hospital, Kodaira, Tokyo 187-8551, Japan.
1）兼　医療法人啓信会京都四条病院パーキンソン病・神経難病センター〔〒600-8481　京都府京都市下京区東堀川通り四条下る四条堀川町272-6〕

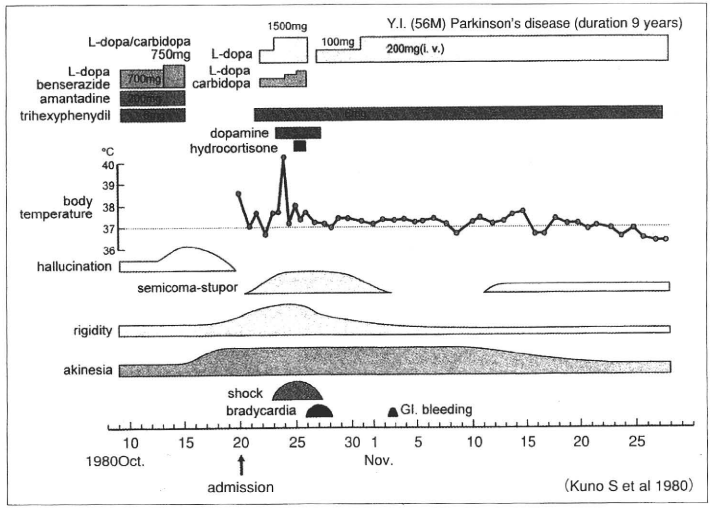

図1　幻覚・妄想を伴い，Parkinson病薬の自己中止によって発症した56歳男性の臨床経過（典型例）

投与量はまったく変えないのに発症した症例を経験したので，そのうちの2症例を呈示する．図2に示すようにこの男性患者は30歳で発症し，27年間の罹病期間を有する進行期例である．彼は，精神症状も一切なく薬の中断もない患者であり，悪性症候群発症時に L-dopa 600mg＋carbidopa 60mg, pergolide 2 mg, droxidopa 1,200mg, amantadine 150mgを1日量として服用していた．ある年の8月の初め，散歩中に倒れているのを発見され入院となった．40℃の高熱と高CK血症（CK：12,500IU nl＜200）を認め悪性症候群を疑い，ただちに生理食塩水の大量点滴と全身の冷却を行った．経口薬は発症前と同じものを同量投与し1週間後回復した．この症例は熱射病と紛らわしい状況であり，完全には熱射病との鑑別は不可能であると思われるが，散歩に出かけたのは早朝であり太陽が出ている日中ではなかったことと，比較的大量の抗PD剤を服用していたことから，悪性症候群様状態と解釈した．

もう1例は，図3[7]に示すようにまだ生理がある40歳代の女性例で，on時には激しい全身の舞踏病様不随意運動をきたす患者が，生理の直前に発熱とPD症状の増悪，高CK血症をきたし，生理が始まると解熱し，運動症状の改善とCK値の低下を生じていた．本例も第2例と同様に抗PD剤の変更はまったくなかったが，女性ホルモンとの関連でPD症状とジスキネジアが連動して変動し，off時に悪性症候群様症状をきたしたものと解釈した．

3．PD患者の悪性症候群の発症機序[8]

第1例のようにPD患者の進行期例で幻覚性精神症状が強く，その時点での断薬は，統合失調症患者に大量のドパミン受容体遮断性抗精神病薬を投与したときと同様の状況となったと解釈される．いい換えれば，PD脳ではドパミン枯渇状況からドパミン作動薬の大量投与によってドパミン受容体刺激過剰状態に変わり，さらに断薬で元の枯渇状態へ戻るという玉突き現象が生じ，結果として視床下部，線条体，辺縁系でのドパミン受容体機能の破綻を生じて悪性症候群が発症すると解釈される．病態機序として視床下部系，黒質線条体系，中脳辺縁系において，ドパミン受容体の機能低下から亢進状態にあったものが急激な機能低下状態に曝されたことが原因と推定される．また，第2,3例では，患者自身の環境変化に対する遺伝的脆弱性などさまざまな要因が関与している可能性がある．PD患

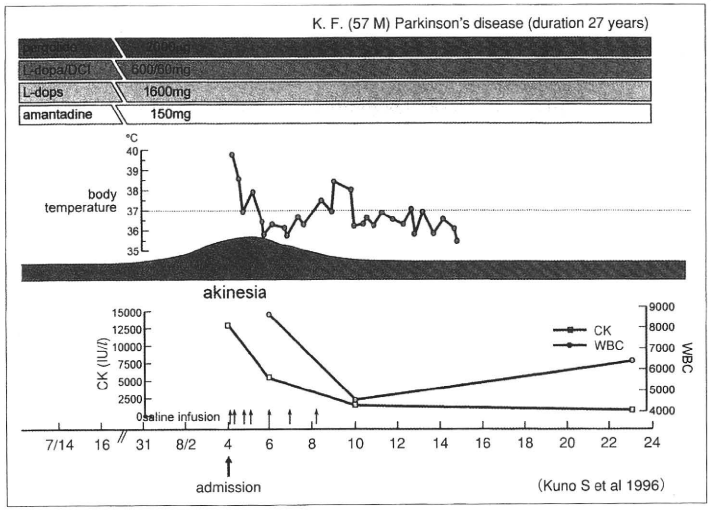

図2　長期罹病期間を有し，大量の抗Parkinson病薬服用中に発症した57歳男性の臨床経過（非典型例）

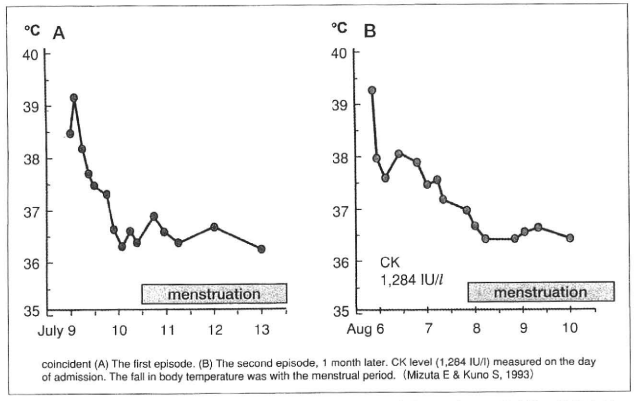

coincident (A) The first episode. (B) The second episode, 1 month later. CK level (1,284 IU/l) measured on the day of admission. The fall in body temperature was with the menstrual period. (Mizuta E & Kuno S, 1993)

図3　激しいジスキネジア，日内変動を有し，抗Parkinson病薬服用中の45歳女性に月経直前に発症した経過（非典型例）